EXACT SOLUTION FOR RIEMANN PROBLEMS OF THE SHEAR SHALLOW WATER MODEL

BONIFACE NKONGA[1] AND PRAVEEN CHANDRASHEKAR[2,*]

Abstract. The shear shallow water model is a higher order model for shallow flows which includes some shear effects that are neglected in the classical shallow models. The model is a non-conservative hyperbolic system which can admit shocks, rarefactions, shear and contact waves. The notion of weak solution is based on a path but the choice of the correct path is not known for this problem. In this paper, we construct exact solution for the Riemann problem assuming a linear path in the space of conserved variables, which is also used in approximate Riemann solvers. We compare the exact solutions with those obtained from a path conservative finite volume scheme on some representative test cases.

1. INTRODUCTION

In the present paper we investigate the solutions of Riemann problems for a non-linear, non-conservative hyperbolic system of equations arising in the modeling of shear shallow water (SSW) flows. In the framework of non-conservative hyperbolic systems, the notion of weak solutions and associated jump conditions need to be revisited. Indeed, in this context, we have to deal with non-classical multiplication of distributions that prevent unique derivation of jump conditions. The path-conservative approach is now a useful tool for numerical approximation of non-conservative hyperbolic systems. The main principle behind this approach is to define the weak solution by assuming some path between two states and derive generalized jump conditions. The paper Volpert [29] is the first to formulate a meaning to non-conservative products using Borel measures. In Dal Maso *et al.* [11], the notion of path is introduced and generalizes the results of Volpert [29]. The first numerical applications resulting from these theoretical analyses are realized in Toumi [28] in the context of Roe scheme for real gases and two-phase flow model, and was generalized under the designation of "path conservative methods" in Parés [23]. Since then, the "path conservative methods" have been widely applied for the numerical solution of non-conservative hyperbolic problems [6,7,12,13,25]. Nevertheless, contrary to the Lax–Wendroff theorem [20] for conservative hyperbolic systems, there is no adequate mathematical theory that can ensure the numerical convergence for any non-conservative system. In the presence of discontinuities, numerical approximations may

---

[1] Université Côte d'Azur, INRIA, CNRS and LJAD, 06108 Nice Cedex 2, France.

[2] Centre for Applicable Mathematics, Tata Institute of Fundamental Research, Bangalore 560065, India.

*Corresponding author: praveen@math.tifrbng.res.in

not converge to the specified entropic weak solution. The equivalent equation of a path conservative scheme based on Lax–Friedrich scheme is examined in Castro *et al.* [5]. Quoting from Castro *et al.* [5], *the difficulty comes from the fact that, unlike the conservative case, the vanishing viscosity limits depend on the regularization of the problem. Even if, for simplicity, we have only calculated the modified equations corresponding to the Lax–Friedrichs scheme, the same difficulty would be present for any other scheme involving a numerical viscous term: the numerical solutions approximate the vanishing viscosity limit of a modified equation whose regularization terms depend both on the chosen family of paths and on the specific form of its viscous terms.* Therefore, there is always a doubt about the ability of numerical strategies to produce relevant numerical solutions that can converge, by mesh refinement, towards a single limit solution. In Abgrall and Karni [1], the following question was pointed out: *once a path is specified and a consistent path-conservative scheme designed, does the numerical solution converge to the assumed path.* They also point out that in some contexts there is clearly a failure of convergence upon grid refinement. In order to clarify the questions that arise in numerical simulations of non-conservative hyperbolic problems, it is necessary to construct exact solutions for a fixed path. From there, we can use the same path in a numerical approach and study if we have a convergence of the numerical solution to the analytical solution. Let us note that attempts to answer these questions exist in the literature for a model of elastodynamics described by a 2×2 non-hyperbolic system. For this model, theoretical analyses and numerical investigations are proposed [8,10], and we even have exact solutions for the Riemann problem [19].

In this paper, we consider an example of a non-conservative hyperbolic system, the shear shallow water model, for which approximate Riemann solver based methods have been developed in the literature [3,9,15] and for which we construct the exact Riemann solution in this work. Riemann solvers are an important building block of modern numerical schemes for hyperbolic systems. Therefore, there can be some confidence when using this approach for more complex data setting [3,9,15]. In the coming sections we will first describe the equations for shear shallow water flows written in a specific non-conservative form. This formulation uses the set of quasi-conservative variables which is very similar to the 10-moment equations of gas dynamics [22], but the system is genuinely non-conservative. Then the path-conservative jump conditions are recalled and used to derive an exact solution of a Riemann problem. Finally, we discuss the convergence of the numerical solution obtained from a path conservative approximate Riemann solver [9] toward the designed exact solution for some representative test cases.

2. The SSW model

The system describing multi-dimensional shear shallow water flow was derived by Teshukov [26] by depth averaging the incompressible Euler equations. This system of equations describes the evolution of the fluid depth h, the depth averaged horizontal velocity $\boldsymbol{v}$ and the Reynolds tensor $\mathcal{P}$, and can be written as [15]

$$\frac{\partial h}{\partial t} + \nabla \cdot (h\boldsymbol{v}) = 0$$

$$\frac{\partial (h\boldsymbol{v})}{\partial t} + \nabla \cdot \left(h\boldsymbol{v} \otimes \boldsymbol{v} + \frac{1}{2}gh^2 I + h\mathcal{P} \right) = -gh\nabla \mathrm{b} - C_f |\boldsymbol{v}|\boldsymbol{v} \tag{2.1}$$

$$\frac{\partial \mathcal{P}}{\partial t} + \boldsymbol{v} \cdot \nabla \mathcal{P} + (\nabla \boldsymbol{v})\mathcal{P} + \mathcal{P}(\nabla \boldsymbol{v})^\top = \mathcal{D}.$$

The tensor $\mathcal{P}$ is symmetric and positive definite; it measures the distortion of the instantaneous horizontal velocity with respect to the depth average velocity $\boldsymbol{v}$. The system derived in Teshukov [26] was non-dissipative ($C_f = 0$, $\mathcal{D} = 0$); in Gavrilyuk *et al.* [15], the modeling of dissipation process was introduced for the evolution of the momentum and the Reynolds stress tensor. The dissipation model provides a closure to the averaging process and was designed such as to preserve the positive definite-ness of the tensor $\mathcal{P}$. Recently [9], the dissipative model proposed in Gavrilyuk *et al.* [15] has been reformulated for the evolution of the energy tensor E. In this context, the SSW model can be written in an almost conservative form. To do this, we define the symmetric

tensors

$$\mathcal{R}_{ij} := h\mathcal{P}_{ij}, \quad \mathcal{E}_{ij} := \frac{1}{2}\mathcal{R}_{ij} + \frac{1}{2}hv_iv_j, \quad 1 \le i, j \le 2.$$

Then, the set of equations for the SSW model (2.1) can be written as follows

$$\frac{\partial \boldsymbol{U}}{\partial t} + \frac{\partial \boldsymbol{F}_1}{\partial x_1} + \frac{\partial \boldsymbol{F}_2}{\partial x_2} + \boldsymbol{B}_1 \frac{\partial h}{\partial x_1} + \boldsymbol{B}_2 \frac{\partial h}{\partial x_2} = \boldsymbol{S} \tag{2.2}$$

where

$$\boldsymbol{U} = \begin{bmatrix} h \\ hv_1 \\ hv_2 \\ \mathcal{E}_{11} \\ \mathcal{E}_{12} \\ \mathcal{E}_{22} \end{bmatrix}, \quad \boldsymbol{F}_1 = \begin{bmatrix} hv_1 \\ \mathcal{R}_{11} + hv_1^2 + \frac{1}{2}gh^2 \\ \mathcal{R}_{12} + hv_1v_2 \\ (\mathcal{E}_{11} + \mathcal{R}_{11})v_1 \\ \mathcal{E}_{12}v_1 + \frac{1}{2}(\mathcal{R}_{11}v_2 + \mathcal{R}_{12}v_1) \\ \mathcal{E}_{22}v_1 + \mathcal{R}_{12}v_2 \end{bmatrix}, \quad \boldsymbol{F}_2 = \begin{bmatrix} hv_2 \\ \mathcal{R}_{12} + hv_1v_2 \\ \mathcal{R}_{22} + hv_2^2 + \frac{1}{2}gh^2 \\ \mathcal{E}_{11}v_2 + \mathcal{R}_{12}v_1 \\ \mathcal{E}_{12}v_2 + \frac{1}{2}(\mathcal{R}_{12}v_2 + \mathcal{R}_{22}v_1) \\ (\mathcal{E}_{22} + \mathcal{R}_{22})v_2 \end{bmatrix},$$

$$\boldsymbol{B}_1 = \begin{bmatrix} 0 \\ 0 \\ 0 \\ ghv_1 \\ \frac{1}{2}ghv_2 \\ 0 \end{bmatrix}, \quad \boldsymbol{B}_2 = \begin{bmatrix} 0 \\ 0 \\ 0 \\ 0 \\ \frac{1}{2}ghv_1 \\ ghv_2 \end{bmatrix}, \quad \boldsymbol{S} = \begin{bmatrix} 0 \\ -gh\frac{\partial \mathrm{b}}{\partial x_1} - C_f|\boldsymbol{v}|v_1 \\ -gh\frac{\partial \mathrm{b}}{\partial x_2} - C_f|\boldsymbol{v}|v_2 \\ -ghv_1\frac{\partial \mathrm{b}}{\partial x_1} + \frac{1}{2}h\mathcal{D}_{11} - C_f|\boldsymbol{v}|v_1^2 \\ -\frac{1}{2}ghv_2\frac{\partial \mathrm{b}}{\partial x_1} - \frac{1}{2}ghv_1\frac{\partial \mathrm{b}}{\partial x_2} + \frac{1}{2}h\mathcal{D}_{12} - C_f|\boldsymbol{v}|v_1v_2 \\ -ghv_2\frac{\partial \mathrm{b}}{\partial x_2} + \frac{1}{2}h\mathcal{D}_{22} - C_f|\boldsymbol{v}|v_2^2 \end{bmatrix}.$$

In the present work, we assume that the bottom topography $\mathrm{b} \equiv \mathrm{b}(x_1, x_2)$ is a given smooth function. The solution must satisfy some positivity constraints which leads to the following solution space for physically admissible solutions

$$\mathcal{U}_{\mathrm{ad}} = \left\{ \boldsymbol{U} \in \mathbb{R}^6 : h > 0, \quad \mathcal{R} > 0 \right\}$$

where $\mathcal{R} > 0$ means that the symmetric tensor $\mathcal{R}$ must be positive definite. We next consider some properties of this model.

2.1. Total energy equation

The additional conservation laws satisfied by the SSW model have been investigated in Gavrilyuk *et al.* [15]. The first one is related to the energy and can be derived as follows. Multiply h equation by $g(h + \mathrm{b})$ and add it to the $\mathcal{E}_{11}$ and $\mathcal{E}_{22}$ equations to obtain

$$\frac{\partial E}{\partial t} + \frac{\partial}{\partial x_1}\left[\left(E + \mathcal{R}_{11} + \frac{1}{2}gh^2\right)v_1 + \mathcal{R}_{12}v_2\right] + \frac{\partial}{\partial x_2}\left[\left(E + \mathcal{R}_{22} + \frac{1}{2}gh^2\right)v_2 + \mathcal{R}_{12}v_1\right] = -C_f|\boldsymbol{v}|^3 + \frac{1}{2}h\operatorname{trace}(\mathcal{D}) \tag{2.3}$$

where the *total energy* is defined as

$$E = \mathcal{E}_{11} + \mathcal{E}_{22} + \frac{1}{2}gh^2 + gh\mathrm{b} = \frac{1}{2}\operatorname{trace}(\mathcal{R}) + \frac{1}{2}h|\boldsymbol{v}|^2 + \frac{1}{2}gh^2 + gh\mathrm{b}. \tag{2.4}$$

The quantity $E = E(\boldsymbol{U})$ is a convex function but it is not a strictly convex function since it has no dependence on $\mathcal{E}_{12}$, and so it cannot serve as an entropy function.

2.2. Entropy equation

We can define the specific entropy

$$s = \frac{\det \mathcal{P}}{h^2} \tag{2.5}$$

which satisfies the equation ([15], Eq. (31))

$$\frac{\partial s}{\partial t} + \boldsymbol{v} \cdot \nabla s = \frac{1}{h^2}[\text{trace}(\mathcal{P})\,\text{trace}(\mathcal{D}) - \text{trace}(\mathcal{P}\mathcal{D})].$$

The above equation can be rewritten as an entropy balance law,

$$\frac{\partial \eta}{\partial t} + \nabla \cdot (\boldsymbol{v}\eta) = -\frac{1}{hs}[\text{trace}(\mathcal{P})\,\text{trace}(\mathcal{D}) - \text{trace}(\mathcal{P}\mathcal{D})]$$

where

$$\eta = \eta(\boldsymbol{U}) = -h\log s = -h\log\left(\frac{\det \mathcal{P}}{h^2}\right)$$

is a convex function of $\boldsymbol{U}$ [21]. Smooth solutions in the absence of dissipation $\mathcal{D}$ satisfy the entropy conservation law. In general, when the solution is not smooth, we require an entropy inequality

$$\frac{\partial \eta}{\partial t} + \nabla \cdot (\boldsymbol{v}\eta) \leq 0$$

to hold in the sense of distributions. For a scalar problem, the entropy condition serves to enforce uniqueness of weak solutions but this is an open problem for systems of conservation laws. However, it is important to satisfy the entropy condition since it is a fundamental property of all natural systems. The availability of such an entropy condition for the SSW model (2.2) indicates that it can serve as a useful mathematical form for the construction of numerical schemes.

Remark 2.1. For a different but related PDE model for shear shallow flows, we refer the reader to Busto *et al.* [4] where a new matrix variable $\mathcal{Q}$ is introduced such that $\mathcal{P} = \mathcal{Q}\mathcal{Q}^\top$. Unlike $\mathcal{P}$, the matrix $\mathcal{Q}$ is not assumed to be symmetric which introduces an extra variable into the model. An equation for $\mathcal{Q}$ is derived under some simplifying assumptions on the rotation of Reynolds tensor by friction forces, whose evolution ensures positivity of $\mathcal{P}$. The total energy E becomes a convex function in terms of the new set of variables $(h, h\boldsymbol{v}, h\mathcal{Q})$, leading to a thermodynamically consistent model. A numerical approach based on path conservative idea is developed, which under the assumption of exact integration of some quantities, leads to a first order semi-discrete scheme which is shown to conserve the total energy, is consistent with the entropy inequality and with the vanishing viscosity limit of the model. In order to ensure the conservation of total energy in the inviscid case for the fully discrete scheme, a scaling of the variable $\mathcal{Q}$ is performed after each time step.

2.3. Hyperbolicity

We will consider the 1-D SSW model which can be written as

$$\frac{\partial \boldsymbol{U}}{\partial t} + \frac{\partial \boldsymbol{F}(\boldsymbol{U})}{\partial x} + \boldsymbol{B}(\boldsymbol{m})\frac{\partial h}{\partial x} = \boldsymbol{S}(\boldsymbol{U}) \tag{2.6}$$

where $\boldsymbol{F} = \boldsymbol{F}_1$, $\boldsymbol{B} = \boldsymbol{B}_1$, $\boldsymbol{m} = h\boldsymbol{v}$, and the source term is given by

$$\boldsymbol{S} = \begin{bmatrix} 0 \\ -gh\frac{\partial \text{b}}{\partial x} - C_f|\boldsymbol{v}|v_1 \\ -C_f|\boldsymbol{v}|v_2 \\ -\alpha|\boldsymbol{v}|^3\mathcal{P}_{11} - ghv_1\frac{\partial \text{b}}{\partial x} - C_f|\boldsymbol{v}|v_1^2 \\ -\alpha|\boldsymbol{v}|^3\mathcal{P}_{12} - \frac{1}{2}ghv_2\frac{\partial \text{b}}{\partial x} - C_f|\boldsymbol{v}|v_1v_2 \\ -\alpha|\boldsymbol{v}|^3\mathcal{P}_{22} - C_f|\boldsymbol{v}|v_2^2 \end{bmatrix}.$$

Ignoring the source term in (2.6) for the moment as they do not contain derivatives of $\boldsymbol{U}$, let us write the non-conservative system (2.6) in quasi-linear form as

$$\frac{\partial \boldsymbol{U}}{\partial t} + \boldsymbol{A}(\boldsymbol{U})\frac{\partial \boldsymbol{U}}{\partial x} = 0, \quad \boldsymbol{A} = \boldsymbol{F}'(\boldsymbol{U}) + \begin{bmatrix} 0 & 0 & 0 & 0 & 0 & 0 \\ 0 & 0 & 0 & 0 & 0 & 0 \\ 0 & 0 & 0 & 0 & 0 & 0 \\ ghv_1 & 0 & 0 & 0 & 0 & 0 \\ \frac{1}{2}ghv_2 & 0 & 0 & 0 & 0 & 0 \\ 0 & 0 & 0 & 0 & 0 & 0 \end{bmatrix}. \tag{2.7}$$

For simplicity of notation, we will sometimes write the velocity components as $(u, v) = (v_1, v_2)$. The system of equations (2.7) is a hyperbolic system with eigenvalues of $\boldsymbol{A}$ being given by Gavrilyuk *et al.* [15] and Berthon *et al.* [2]

$$\lambda_1 = u - \sqrt{gh + 3\mathcal{P}_{11}}, \quad \lambda_2 = u - \sqrt{\mathcal{P}_{11}}, \quad \lambda_3 = \lambda_4 = u, \quad \lambda_5 = u + \sqrt{\mathcal{P}_{11}}, \quad \lambda_6 = u + \sqrt{gh + 3\mathcal{P}_{11}}.$$

The first and last eigenvalues correspond to genuinely non-linear characteristic fields in the sense of Lax [17], while the remaining eigenvalues correspond to linearly degenerate characteristic fields [15]. Hence λ_1, λ_6 are associated with shock/rarefaction waves while the remaining eigenvalues give rise to shear/contact waves. To study the hyperbolicity, it is useful to transform the equations in terms of primitive variables

$$\boldsymbol{Q} = [h, \ v_1, \ v_2, \ \mathcal{P}_{11}, \ \mathcal{P}_{12}, \ \mathcal{P}_{22}]$$

as the independent variables. Define

$$\text{A} = \sqrt{gh + 3\mathcal{P}_{11}}, \quad \text{C} = \sqrt{\mathcal{P}_{11}}.$$

Then the eigenvectors in terms of the primitive variables are give as follows.
1-wave: shock/rarefaction: $\lambda_1 = u - \text{A}$

$$\boldsymbol{r}_1 = \left[h\left(\text{A}^2 - \text{C}^2\right), \ -\text{A}\left(\text{A}^2 - \text{C}^2\right), \ -2\text{A}\mathcal{P}_{12}, \ 2\text{C}^2\left(\text{A}^2 - \text{C}^2\right), \ \left(\text{A}^2 + \text{C}^2\right)\mathcal{P}_{12}, \ 4\mathcal{P}_{12}^2\right].$$

2-shear wave: $\lambda_2 = u - \text{C}$

$$\boldsymbol{r}_2 = \left[0, \ 0, \ -\text{C}, \ 0, \ \text{C}^2, \ 2\mathcal{P}_{12}\right]^\top.$$

3,4-contact wave: $\lambda_3 = \lambda_4 = u$

$$\boldsymbol{r}_3 = [0, \ 0, \ 0, \ 0, \ 0, \ 1]^\top$$
$$\boldsymbol{r}_4 = [-h, \ 0, \ 0, \ gh + \mathcal{P}_{11}, \ \mathcal{P}_{12}, \ 0].$$

5-shear wave: $\lambda_5 = u + \text{C}$

$$\boldsymbol{r}_5 = \left[0, \ 0, \ \text{C}, \ 0, \ \text{C}^2, \ 2\mathcal{P}_{12}\right]^\top.$$

6-wave: shock/rarefaction: $\lambda_6 = u + \text{A}$

$$\boldsymbol{r}_6 = \left[h\left(\text{A}^2 - \text{C}^2\right), \ \text{A}\left(\text{A}^2 - \text{C}^2\right), \ 2\text{A}\mathcal{P}_{12}, \ 2\text{C}^2\left(\text{A}^2 - \text{C}^2\right), \ \left(\text{A}^2 + \text{C}^2\right)\mathcal{P}_{12}, \ 4\mathcal{P}_{12}^2\right].$$

The waves and their ordering are illustrated in Figure 1. Note that, when $\mathcal{P}_{11}$ goes to zero, we have $\text{C} \to 0$ and the system is no more hyperbolic. Indeed, the eigenvectors $\boldsymbol{r}_2$, $\boldsymbol{r}_3$ and $\boldsymbol{r}_5$ become dependent. Moreover, even if for $\mathcal{P}_{11} = \mathcal{P}_{12} = \mathcal{P}_{22} = 0$ the system (2.7) can be formally reduced to a conservative formulation, this change in the nature of the model is accompanied here by an eigenvalue whose multiplicity becomes four but asymptotically associated to only two independent eigenvectors.
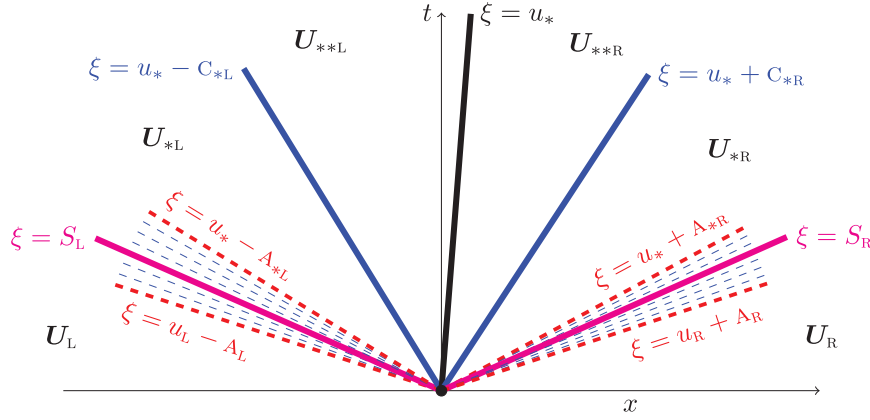
FIGURE 1. Shear shallow water model: Wave pattern for the 1-D Riemann problem. Plain lines are used for discontinuities and dashed lines for rarefaction waves. For the first and the last waves, we need to estimate whether it is a shock or a rarefaction wave. Waves speeds are defined with the self-similar variable $\xi = x/t$.

3. CONCEPT OF WEAK SOLUTION

If we have discontinuous solutions for (2.7), then we have to give a proper mathematical meaning to the spatial derivative term which is based on a weak formulation using integration by parts if $\boldsymbol{A}$ is the gradient of a flux function as in case of conservation laws. If $\boldsymbol{A}$ is not the gradient of a flux, then the non-conservative product is interpreted as a Borel measure [11]. This definition requires the choice of a smooth path $\Psi : [0,1] \times \mathcal{U}_{ad} \times \mathcal{U}_{ad} \to \mathcal{U}_{ad}$ connecting the two states $\boldsymbol{U}_L, \boldsymbol{U}_R$ across the jump discontinuity at $x = x_0$ such that

$$\Psi(0; \boldsymbol{U}_L, \boldsymbol{U}_R) = \boldsymbol{U}_L, \quad \Psi(1; \boldsymbol{U}_L, \boldsymbol{U}_R) = \boldsymbol{U}_R$$

where $\mathcal{U}_{ad}$ is the set of admissible states. Then the non-conservative product is defined as the Borel measure [11, 18]

$$\mu(x_0) = \left[\int_0^1 \boldsymbol{A}(\Psi(\xi; \boldsymbol{U}_L, \boldsymbol{U}_R)) \frac{d\Psi}{d\xi}(\xi; \boldsymbol{U}_L, \boldsymbol{U}_R) d\xi \right] \delta(x_0)$$

where δ is the Dirac delta function. The quantity inside the square brackets will be referred to as the *fluctuation* and plays an important role in the construction of approximate Riemann solvers. This viewpoint is equivalent to the definition of non-conservative product proposed by Volpert [29]. Using this notion, a theory of weak solutions can be developed based on which the Riemann problem has usual structure as for conservative systems, leading to shocks or rarefaction waves corresponding to genuinely non-linear characteristic fields and contact waves corresponding to linearly degenerate fields. Across a point of discontinuity moving with speed S, a weak solution has to satisfy the generalized Rankine–Hugoniot jump condition

$$\int_0^1 [\boldsymbol{A}(\Psi(\xi; \boldsymbol{U}_L, \boldsymbol{U}_R)) - SI] \frac{d\Psi}{d\xi}(\xi; \boldsymbol{U}_L, \boldsymbol{U}_R) d\xi = 0.$$

The choice of the correct path is a difficult question and has to be derived from a regularized model motivated from the physical background of the problem. In many applications, the choice of the correct path is not known and in practice, it is usual to consider the linear path in state space

$$\Psi(\xi; \boldsymbol{U}_L, \boldsymbol{U}_R) = \boldsymbol{U}_L + \xi(\boldsymbol{U}_R - \boldsymbol{U}_L). \tag{3.1}$$

Then the jump condition for our model (2.6) becomes

$$\int_0^1 \boldsymbol{A}(\Psi(\xi; \boldsymbol{U}_L, \boldsymbol{U}_R)) \frac{d\Psi}{d\xi} d\xi = \boldsymbol{F}_R - \boldsymbol{F}_L + \boldsymbol{B}(\boldsymbol{m}_L, \boldsymbol{m}_R)(h_R - h_L) = S(\boldsymbol{U}_R - \boldsymbol{U}_L) \tag{3.2}$$

where

$$\boldsymbol{B}(\boldsymbol{m}_L, \boldsymbol{m}_R) = \boldsymbol{B}\left(\frac{\boldsymbol{m}_L + \boldsymbol{m}_R}{2}\right).$$

The source term $\boldsymbol{S}$ does not make any contribution to the jump conditions since it does not contain derivative of $\boldsymbol{U}$.

3.1. Rankine–Hugoniot jump conditions

In the following, we will assume that $\boldsymbol{U}_L, \boldsymbol{U}_R$ are the left and right states in a Riemann problem. Let us define the average and jump operators by

$$\{\!\!\{\cdot\}\!\!\} = \frac{(\cdot)_L + (\cdot)_R}{2}, \quad [\![\cdot]\!] = (\cdot)_R - (\cdot)_L.$$

Then the jump conditions (3.2) across a discontinuity moving with speed S lead to the following set of generalized Rankine–Hugoniot conditions.

$$[\![hu]\!] = S[\![h]\!] \tag{3.3a}$$

$$\left[\!\!\left[\mathcal{R}_{11} + hu^2 + \frac{1}{2}gh^2\right]\!\!\right] = S[\![hu]\!] \tag{3.3b}$$

$$[\![\mathcal{R}_{12} + huv]\!] = S[\![hv]\!] \tag{3.3c}$$

$$[\![\mathcal{E}_{11}u + \mathcal{R}_{11}u]\!] + g\{\!\!\{hu\}\!\!\}[\![h]\!] = S[\![\mathcal{E}_{11}]\!] \tag{3.3d}$$

$$\left[\!\!\left[\mathcal{E}_{12}u + \frac{1}{2}(\mathcal{R}_{11}v + \mathcal{R}_{12}u)\right]\!\!\right] + \frac{1}{2}g\{\!\!\{hv\}\!\!\}[\![h]\!] = S[\![\mathcal{E}_{12}]\!] \tag{3.3e}$$

$$[\![\mathcal{E}_{22}u + \mathcal{R}_{12}v]\!] = S[\![\mathcal{E}_{22}]\!]. \tag{3.3f}$$

Moreover, the total energy equation (2.3) also has an associated jump condition.

Lemma 3.1. *For the linear path* (3.1), *the jump conditions* (3.3a)–(3.3f) *are consistent with the jump conditions of the total energy equation* (2.3).

Proof. We will show that the jump conditions (3.3a)–(3.3f) imply that

$$\left[\!\!\left[\left(E + \mathcal{R}_{11} + \frac{1}{2}gh^2\right)u + \mathcal{R}_{12}v\right]\!\!\right] = S[\![E]\!] \tag{3.4}$$

which is the jump condition for the total energy equation. Adding the jump conditions from $\mathcal{E}_{11}, \mathcal{E}_{22}$ equations

$$[\![(\mathcal{E}_{11} + \mathcal{E}_{22})u + \mathcal{R}_{11}u + \mathcal{R}_{12}v]\!] + g\{\!\!\{hu\}\!\!\}[\![h]\!] = S[\![\mathcal{E}_{11} + \mathcal{E}_{22}]\!]. \tag{3.5}$$

Also

$$\begin{aligned}
[\![(gh^2 + gh\mathrm{b})u]\!] &= g\{\!\!\{hu\}\!\!\}[\![h]\!] + g\{\!\!\{h\}\!\!\}[\![hu]\!] + g\mathrm{b}[\![hu]\!] \\
&= g\{\!\!\{hu\}\!\!\}[\![h]\!] + Sg\{\!\!\{h\}\!\!\}[\![h]\!] + Sg\mathrm{b}[\![h]\!], \quad \text{using (3.3a)} \\
&= g\{\!\!\{hu\}\!\!\}[\![h]\!] + S\left[\!\!\left[\frac{1}{2}gh^2 + gh\mathrm{b}\right]\!\!\right].
\end{aligned} \tag{3.6}$$

Adding (3.5) and (3.6), we obtain (3.4). $\qquad\square$

4. PROPERTIES AND STRUCTURES OF SINGLE WAVES

We will focus in this paper on the derivation of an exact solution for the Riemann problem associated to the 1-D SSW model where the source term is set to zero. The spectral analysis of this genuinely non-conservative hyperbolic system was proposed in Gavrilyuk *et al.* [15]. Within the *path conservative* framework, generalized jump conditions for this non-conservative system was derived in Chandrashekar *et al.* [9]. These results have been recalled in the previous section. In order to define the strategy that will allow us to obtain the exact solution of the Riemann problem, we first need to characterize the properties of waves associated with each eigenvalue. The first and the sixth characteristic fields, respectively associated to $\lambda_1 = u - \mathrm{A}$ and $\lambda_6 = u + \mathrm{A}$, are genuinely non-linear and can develop either shock (discontinuous) or rarefaction (continuous) waves. The other characteristic fields are associated to linearly degenerate waves. We will name *contact wave* the field associated to the eigenvalue $\lambda_3 = \lambda_4 = u$ and *shear waves* the field associated to $\lambda_2 = u - \mathrm{C}$ and $\lambda_5 = u + \mathrm{C}$. Asymptotically, the contact and the shear waves will collapse to a single wave when C goes to zero, which will be the case when the variable $\mathcal{P}_{11}$ goes to zero. Since the tensor $\mathcal{P}$ is always symmetric and positive definite, there is a strict ordering of the eigenvalues

$$u - \mathrm{A} < u - \mathrm{C} < u < u + \mathrm{C} < u + \mathrm{A}.$$

However, when approximations are applied with small values of $\mathcal{P}_{11}$, we can face some numerical inconsistencies. Riemann invariants are constant across linearly degenerate waves and rarefaction waves, whereas for shock waves, generalized jump conditions should be satisfied. In the subsequent subsections, we will derive the Riemann invariants or the relations to be satisfied for each single wave connecting two different states: the state $\boldsymbol{U}_{\mathrm{L}}$ on the left and $\boldsymbol{U}_{\mathrm{R}}$ on the right of the wave.

4.1. Rarefaction waves

The eigenvalues $\lambda_1 = u - \mathrm{A}$ and $\lambda_6 = u + \mathrm{A}$ are genuinely non-linear and may give rise to rarefaction waves.

Theorem 4.1. *For the 1-rarefaction wave, the Riemann invariants are given by*

$$\frac{\mathcal{P}_{11}}{h^2}, \quad u + \mathfrak{a}(h, c), \quad \frac{\det(\mathcal{P})}{h^2}, \quad \frac{\mathcal{P}_{12}}{gh + 2\mathcal{P}_{11}}, \quad v + \frac{2\mathcal{P}_{12}}{gh + 2\mathcal{P}_{11}}\mathfrak{a}(h, c) \tag{4.1}$$

and for the 6-rarefaction wave, the Riemann invariants are given by

$$\frac{\mathcal{P}_{11}}{h^2}, \quad u - \mathfrak{a}(h, c), \quad \frac{\det(\mathcal{P})}{h^2}, \quad \frac{\mathcal{P}_{12}}{gh + 2\mathcal{P}_{11}}, \quad v - \frac{2\mathcal{P}_{12}}{gh + 2\mathcal{P}_{11}}\mathfrak{a}(h, c) \tag{4.2}$$

where

$$\mathfrak{a}(h, c) = \sqrt{gh + 3ch^2} + \frac{g}{\sqrt{3c}}\sinh^{-1}\sqrt{\frac{3ch}{g}}, \quad c = \frac{\mathcal{P}_{11}}{h^2}. \tag{4.3}$$

Proof. We find the Riemann invariants by analyzing the integrals curves of the eigenvector fields. The integral curve corresponding to $\boldsymbol{r}_1$ satisfy the following set of equations

$$\frac{\mathrm{d}h}{h(\mathrm{A}^2 - \mathrm{C}^2)} = \frac{\mathrm{d}u}{-\mathrm{A}(\mathrm{A}^2 - \mathrm{C}^2)} = \frac{\mathrm{d}v}{-2\mathrm{A}\mathcal{P}_{12}} = \frac{\mathrm{d}\mathcal{P}_{11}}{2\mathrm{C}^2(\mathrm{A}^2 - \mathrm{C}^2)} = \frac{\mathrm{d}\mathcal{P}_{12}}{(\mathrm{A}^2 + \mathrm{C}^2)\mathcal{P}_{12}} = \frac{\mathrm{d}\mathcal{P}_{22}}{4\mathcal{P}_{12}^2}. \tag{4.4}$$

Using the first and fourth terms in (4.4), we get

$$\frac{\mathrm{d}h}{h} = \frac{\mathrm{d}\mathcal{P}_{11}}{2\mathcal{P}_{11}} \quad \implies \quad \frac{\mathcal{P}_{11}}{h^2} = \frac{\mathcal{R}_{11}}{h^3} = \text{constant} = c$$

which is the first invariant. Using the first and second terms in (4.4), we get

$$\mathrm{d}u = -\frac{\mathrm{A}}{h}\mathrm{d}h = -\frac{\sqrt{gh + 3ch^2}}{h}\mathrm{d}h$$

where we used the first invariant. Integrating this, we obtain the second invariant $u + \mathfrak{a}(h, c)$, with

$$\mathfrak{a}(h, c) = \int \frac{1}{h}\sqrt{gh + 3ch^2}\mathrm{d}h \equiv \sqrt{gh + 3ch^2} + \frac{g}{\sqrt{3c}}\sinh^{-1}\sqrt{\frac{3ch}{g}}.$$

By definition of the determinant, we have $\det(\mathcal{P}) = \mathcal{P}_{11}\mathcal{P}_{22} - \mathcal{P}_{12}^2$. Therefore,

$$\begin{aligned}
\mathrm{d}[\det(\mathcal{P})] &= \mathcal{P}_{22}\mathrm{d}\mathcal{P}_{11} + \mathcal{P}_{11}\mathrm{d}\mathcal{P}_{22} - 2\mathcal{P}_{12}\mathrm{d}\mathcal{P}_{12} \\
&= \mathcal{P}_{22}\frac{2\mathrm{C}}{h}\mathrm{d}h + \mathcal{P}_{11}\frac{4\mathcal{P}_{12}^2}{h(\mathrm{A}^2 - \mathrm{C}^2)}\mathrm{d}h - 2\mathcal{P}_{12}\frac{(\mathrm{A}^2 + \mathrm{C}^2)\mathcal{P}_{12}}{h(\mathrm{A}^2 - \mathrm{C}^2)}\mathrm{d}h = 2\frac{\det(\mathcal{P})}{h}\mathrm{d}h.
\end{aligned}$$

Hence, the enstrophy $\frac{\det(\mathcal{P})}{h^2}$ is conserved across rarefaction waves, which is the third Riemann invariant. From the first and fifth terms in (4.4), we get

$$\mathrm{d}\ln\mathcal{P}_{12} = \frac{1}{h}\frac{\mathrm{A}^2 + \mathrm{C}^2}{\mathrm{A}^2 - \mathrm{C}^2}\mathrm{d}h = \frac{1}{h}\frac{gh + 4\mathcal{P}_{11}}{gh + 2\mathcal{P}_{11}}\mathrm{d}h = \frac{g + 4ch}{gh + 2ch^2}\mathrm{d}h = \mathrm{d}\ln(gh + 2ch^2)$$

and we obtain the fourth invariant, for convenience denoted as $\beta = \frac{\mathcal{P}_{12}}{gh + 2ch^2}$.

Finally, from the first and third terms in (4.4), we get

$$\mathrm{d}v = -\frac{2\mathrm{A}\mathcal{P}_{12}}{h(\mathrm{A}^2 - \mathrm{C}^2)}\mathrm{d}h = -2\beta\frac{\sqrt{gh + 3ch^2}}{h}\mathrm{d}h$$

and integrating this we obtain the fifth invariant: $v - 2\beta\mathfrak{a}(h, c)$. The proof for the 6-rarefaction is similar except for some sign differences. $\square$

The two states $\boldsymbol{U}_\mathrm{L}, \boldsymbol{U}_\mathrm{R}$ can be connected by a rarefaction wave provided they satisfy the Lax condition; for a 1-rarefaction, they must satisfy

$$\lambda_1(\boldsymbol{U}_\mathrm{L}) < \lambda_1(\boldsymbol{U}_\mathrm{R}) \tag{4.5}$$

and a similar condition must be satisfied in case of a 6-rarefaction wave.

Lemma 4.2. *The set of admissible left and right states $\boldsymbol{U}_\mathrm{L}, \boldsymbol{U}_\mathrm{R}$ that can be connected by*

(1) *a 1-rarefaction must satisfy $h_\mathrm{R} < h_\mathrm{L}$.*
(2) *a 6-rarefaction must satisfy $h_\mathrm{L} < h_\mathrm{R}$.*

Proof. (1) Using the Riemann invariants $c = \frac{\mathcal{P}_{11}}{h^2}$ and $u + \mathfrak{a}(h, c)$ the difference of the velocity can be written as

$$\begin{aligned}
u_\mathrm{L} - u_\mathrm{R} &= \mathfrak{a}(h_\mathrm{R}, c) - \mathfrak{a}(h_\mathrm{L}, c) \\
&= \sqrt{gh_\mathrm{R} + 3\mathcal{P}_{11}^\mathrm{R}} - \sqrt{gh_\mathrm{L} + 3\mathcal{P}_{11}^\mathrm{L}} + \frac{g}{\sqrt{3c}}\left[\sinh^{-1}\sqrt{\frac{3ch_\mathrm{R}}{g}} - \sinh^{-1}\sqrt{\frac{3ch_\mathrm{L}}{g}}\right].
\end{aligned}$$

For a 1-rarefaction wave, the characteristic speeds must satisfy the condition (4.5), which leads to

$$u_\mathrm{L} - \sqrt{gh_\mathrm{L} + 3\mathcal{P}_{11}^\mathrm{L}} < u_\mathrm{R} - \sqrt{gh_\mathrm{R} + 3\mathcal{P}_{11}^\mathrm{R}} \implies u_\mathrm{L} - u_\mathrm{R} < \sqrt{gh_\mathrm{L} + 3\mathcal{P}_{11}^\mathrm{L}} - \sqrt{gh_\mathrm{R} + 3\mathcal{P}_{11}^\mathrm{R}}.$$

Combining the above two relations, we get

$$2\sqrt{gh_{\mathrm{R}} + 3ch_{\mathrm{R}}^2} + \frac{g}{\sqrt{3c}}\sinh^{-1}\sqrt{\frac{3ch_{\mathrm{R}}}{g}} \le 2\sqrt{gh_{\mathrm{L}} + 3ch_{\mathrm{L}}^2} + \frac{g}{\sqrt{3c}}\sinh^{-1}\sqrt{\frac{3ch_{\mathrm{L}}}{g}}.$$

On the other hand, the function $f(h,c) = 2\sqrt{gh + 3ch^2} + \frac{g}{\sqrt{3c}}\sinh^{-1}\sqrt{\frac{3ch}{g}}$ is a increasing function of h for c fixed and $g > 0$ a given constant. Therefore, the conditions on the characteristic speeds is satisfied if and only if $h_{\mathrm{R}} < h_{\mathrm{L}}$. The proof is similar for the case of a 6-rarefaction wave. □

4.2. Internal structure of 1-rarefaction

The solution inside the rarefaction is self-similar and depends only on the ratio x/t. The slope of the characteristics is

$$\xi = \frac{x}{t} = u - \mathrm{A} \quad \Longrightarrow \quad -\frac{\mathrm{A}}{h}\mathrm{d}h = \mathrm{d}u = \mathrm{d}\xi + \mathrm{d}\mathrm{A}$$

where equation (4.4) has been used. From this we obtain the relation

$$\mathrm{d}\xi = -\frac{3g + 12ch}{2\sqrt{gh + 3ch^2}}\mathrm{d}h \quad \text{where} \quad c = \frac{\mathcal{P}_{11}^{\mathrm{L}}}{h_{\mathrm{L}}^2}.$$

We can integrate this ODE with the initial condition: $h(\xi_{\mathrm{L}}) = h_{\mathrm{L}}$ and $\xi_{\mathrm{L}} = u_{\mathrm{L}} - \sqrt{gh_{\mathrm{L}} + 3\mathcal{P}_{11}^{\mathrm{L}}}$.

We then obtain

$$\xi - \xi_{\mathrm{L}} = -\Big(\mathfrak{b}(h) - \mathfrak{b}(h_{\mathrm{L}})\Big) \quad \text{with} \quad \mathfrak{b}(h) = 2\sqrt{gh + 3ch^2} + \frac{g}{\sqrt{3c}}\sinh^{-1}\sqrt{\frac{3ch}{g}}.$$

This equation implicitly defines the function $h(\xi)$ in the internal structure of the 1-rarefaction. Once $h = h(\xi)$ is obtained, we can use the Riemann invariants to compute all the other variables inside the rarefaction wave leading to the complete solution $\boldsymbol{U}(\xi)$ for $u_{\mathrm{L}} - \mathrm{A}_{\mathrm{L}} \le \xi \le u_{\mathrm{R}} - \mathrm{A}_{\mathrm{R}}$.

4.3. Shear waves

The eigenvalues λ_2, λ_5 and the associated eigenvectors give rise to shear waves. Across a shear wave, the water depth h and normal velocity u are continuous while the transverse velocity v may have a jump as shown by the Riemann invariants.

Theorem 4.3. *For the 2-shear wave, the Riemann invariants are given by*

$$h, \quad u, \quad \mathcal{P}_{11}, \quad v\sqrt{\mathcal{P}_{11}} + \mathcal{P}_{12}, \quad \det(\mathcal{P})$$

while for the 5-shear wave, they are given by

$$h, \quad u, \quad \mathcal{P}_{11}, \quad v\sqrt{\mathcal{P}_{11}} - \mathcal{P}_{12}, \quad \det(\mathcal{P}).$$

Proof. The integral curve corresponding to the eigenvector $\boldsymbol{r}_2$ satisfies the equations

$$\frac{\mathrm{d}h}{0} = \frac{\mathrm{d}u}{0} = \frac{\mathrm{d}v}{-\mathrm{C}} = \frac{\mathrm{d}\mathcal{P}_{11}}{0} = \frac{\mathrm{d}\mathcal{P}_{12}}{\mathrm{C}^2} = \frac{\mathrm{d}\mathcal{P}_{22}}{2\mathcal{P}_{12}}.$$

We immediately see that $h, u, \mathcal{P}_{11}$ are invariants. From the third and fifth terms, we obtain

$$\mathrm{C}\mathrm{d}v + \mathrm{d}\mathcal{P}_{12} = 0 \quad \Longrightarrow \quad v\sqrt{\mathcal{P}_{11}} + \mathcal{P}_{12} = \text{constant}.$$

Finally from the fifth and sixth terms, we obtain

$$-2\mathcal{P}_{12}\mathrm{d}\mathcal{P}_{12} + \mathrm{C}^2\mathrm{d}\mathcal{P}_{22} = 0 \quad \Longrightarrow \quad \det(\mathcal{P}) = \text{constant}.$$

The proof for the 5-shear wave is similar. □

Remark 4.4. Note that, as h and $\mathcal{P}_{11}$ are Riemann invariants of shear waves, the total pressure $\mathrm{P} = \frac{gh^2}{2} + \mathcal{R}_{11}$ is also invariant across shear waves. Moreover, across the 2-shear wave, the eigenvalue $\lambda_2 = u - \sqrt{\mathcal{P}_{11}}$ is an invariant, and across the 5-shear wave, the eigenvalue $\lambda_5 = u + \sqrt{\mathcal{P}_{11}}$ is an invariant. It can be checked that any two states $\boldsymbol{U}_{\mathrm{L}}, \boldsymbol{U}_{\mathrm{R}}$ which satisfy the Riemann invariants will satisfy all the jump conditions for the shear waves, with the speed of the discontinuity being λ_2 or λ_5.

4.4. Contact waves

The eigenvalues λ_3, λ_4 and the corresponding eigenvectors give rise to contact waves. Across such a wave the velocity is continuous but the water depth may possibly have a jump discontinuity.

Theorem 4.5. *For the contact wave, the Riemann invariants are given by*

$$u, \quad v, \quad \mathcal{R}_{12} \quad \text{and} \quad \mathrm{P} = \frac{gh^2}{2} + \mathcal{R}_{11}$$

where P *is defined as the total pressure.*

Proof. The contact wave is associated to the eigenvalue u with a multiplicity of two with two linearly independent eigenvectors. As the multiplicity is two, we cannot expect more than four Riemann invariants. Indeed, the invariants should satisfy the following equations due to the two eigenvectors $\boldsymbol{r}_3, \boldsymbol{r}_4$,

$$\frac{\mathrm{d}h}{0} = \frac{\mathrm{d}u}{0} = \frac{\mathrm{d}v}{0} = \frac{\mathrm{d}\mathcal{P}_{11}}{0} = \frac{\mathrm{d}\mathcal{P}_{12}}{0} = \frac{\mathrm{d}\mathcal{P}_{22}}{1}$$

and

$$\frac{\mathrm{d}h}{-h} = \frac{\mathrm{d}u}{0} = \frac{\mathrm{d}v}{0} = \frac{\mathrm{d}\mathcal{P}_{11}}{gh + \mathcal{P}_{11}} = \frac{\mathrm{d}\mathcal{P}_{12}}{\mathcal{P}_{12}} = \frac{\mathrm{d}\mathcal{P}_{22}}{0}.$$

As a consequence, the Riemann invariants for contact waves are defined by the following equalities

$$\frac{\mathrm{d}h}{-h} = \frac{\mathrm{d}u}{0} = \frac{\mathrm{d}v}{0} = \frac{\mathrm{d}\mathcal{P}_{11}}{gh + \mathcal{P}_{11}} = \frac{\mathrm{d}\mathcal{P}_{12}}{\mathcal{P}_{12}}.$$

From the second and the third terms of these equalities we obtain the invariants u and v. Combining the first and the fifth terms we find that $\mathcal{R}_{12}$ is the third invariant. Finally, the first and the fourth terms give

$$gh\mathrm{d}h + \mathcal{P}_{11}\mathrm{d}h + h\mathrm{d}\mathcal{P}_{11} = 0 \quad \Longrightarrow \quad \mathrm{d}\left(g\frac{h^2}{2} + h\mathcal{P}_{11}\right) = 0$$

so that $\mathrm{P} = \frac{gh^2}{2} + \mathcal{R}_{11}$ is the fourth invariant. $\qquad\square$

Remark 4.6. By definition, the gradients of these Riemann invariants, with respect to the primitive variable $\boldsymbol{Q}$, are orthogonal to the plane spanned by eigenvectors $\boldsymbol{r}_3$ and $\boldsymbol{r}_4$,

$$\begin{cases} \boldsymbol{r}_3 \cdot \dfrac{\partial u}{\partial \boldsymbol{Q}} = 0 \\ \boldsymbol{r}_4 \cdot \dfrac{\partial u}{\partial \boldsymbol{Q}} = 0 \end{cases}, \quad \begin{cases} \boldsymbol{r}_3 \cdot \dfrac{\partial v}{\partial \boldsymbol{Q}} = 0 \\ \boldsymbol{r}_4 \cdot \dfrac{\partial v}{\partial \boldsymbol{Q}} = 0 \end{cases}, \quad \begin{cases} \boldsymbol{r}_3 \cdot \dfrac{\partial \mathcal{R}_{12}}{\partial \boldsymbol{Q}} = 0 \\ \boldsymbol{r}_4 \cdot \dfrac{\partial \mathcal{R}_{12}}{\partial \boldsymbol{Q}} = 0 \end{cases} \quad \text{and} \quad \begin{cases} \boldsymbol{r}_3 \cdot \dfrac{\partial \mathrm{P}}{\partial \boldsymbol{Q}} = 0 \\ \boldsymbol{r}_4 \cdot \dfrac{\partial \mathrm{P}}{\partial \boldsymbol{Q}} = 0 \end{cases}$$

which can be verified. Moreover, we see that the eigenvalues $\lambda_3 = \lambda_4 = u$ is an invariant.

Remark 4.7. Let us examine the jump conditions for the contact wave. The speed of the contact wave is equal to the common fluid velocity $u_{\mathrm{L}} = u_{\mathrm{R}} = u = \lambda_3 = \lambda_4$ which are linearly degenerate. Then the jump conditions lead to the following set of conditions

$$\left[\!\left[\mathcal{R}_{11} + \frac{1}{2}gh^2\right]\!\right] = 0, \quad [\![\mathcal{R}_{12}]\!] = 0, \quad [\![\mathcal{R}_{11}v]\!] + g\{\!\{hv\}\!\}[\![h]\!] = 0, \quad [\![\mathcal{R}_{12}v]\!] = 0. \tag{4.6}$$

From the first condition, the total pressure P is constant across this wave. From the first and third conditions, we obtain

$$\left(\{\!\{\mathcal{R}_{11}\}\!\} + \frac{1}{4}g[\![h]\!]^2 \right)[\![v]\!] = 0.$$

Since we $\mathcal{R}_{11}$ must be strictly positive, the first factor cannot be zero and hence we require that $[\![v]\!] = 0$, so that both velocity components are continuous across the contact wave. The second condition of (4.6) shows that $\mathcal{R}_{12}$ is also continuous across the middle wave. These results are consistent with the Riemann invariants derived in the previous theorem.

4.5. Shock wave, Hugoniot curve and entropy condition

The states $\boldsymbol{U}_{\mathrm{L}}, \boldsymbol{U}_{\mathrm{R}}$ can be connected by a shock wave only if they satisfy the Lax condition, *i.e.*, the characteristics must intersect into the shock wave. For the 1-shock, this condition is given by

$$\lambda_1(\boldsymbol{U}_{\mathrm{L}}) > S > \lambda_1(\boldsymbol{U}_{\mathrm{R}}) \tag{4.7}$$

where S is the shock speed, with a similar condition for the 6-shock wave. Before using this condition, we derive the Hugoniot relation between the two states which follows from the generalized jump conditions after eliminating the velocity.

Theorem 4.8. *The set of states $\boldsymbol{U}_{\mathrm{L}}, \boldsymbol{U}_{\mathrm{R}}$ which can be connected by a shock lie on the Hugoniot curve given by*

$$\frac{3}{2}[\![\tau \mathcal{R}_{11}]\!] - \{\!\{\tau\}\!\}[\![\mathcal{R}_{11}]\!] + \frac{g[\![\tau]\!]^3}{4\tau_{\mathrm{L}}^2 \tau_{\mathrm{R}}^2} = 0 \quad \text{with} \quad \tau = \frac{1}{h}. \tag{4.8}$$

Proof. Let us change to a coordinate frame in which the shock is stationary. The jump conditions for the continuity, x-momentum and x component of energy equation are

$$[\![hu]\!] = 0, \quad \left[\!\left[\mathcal{R}_{11} + hu^2 + \frac{1}{2}gh^2\right]\!\right] = 0, \quad [\![(\mathcal{E}_{11} + \mathcal{R}_{11})u]\!] + g\{\!\{hu\}\!\}[\![h]\!] = 0.$$

Let $m = h_{\mathrm{L}}u_{\mathrm{L}} = h_{\mathrm{R}}u_{\mathrm{R}}$, then the second and third conditions can be written as

$$[\![\mathcal{R}_{11}]\!] + m[\![u]\!] + g\{\!\{h\}\!\}[\![h]\!] = 0, \quad \frac{3}{2}[\![\mathcal{P}_{11}]\!] + \{\!\{u\}\!\}[\![u]\!] + g[\![h]\!] = 0.$$

Let $\tau = 1/h$; then

$$\{\!\{h\}\!\} = \{\!\{1/\tau\}\!\} = \frac{1}{\tau_{\mathrm{L}}\tau_{\mathrm{R}}}\{\!\{\tau\}\!\}, \quad [\![h]\!] = [\![1/\tau]\!] = -\frac{1}{\tau_{\mathrm{L}}\tau_{\mathrm{R}}}[\![\tau]\!].$$

The two jump conditions become

$$[\![\mathcal{R}_{11}]\!] + m[\![u]\!] - \frac{g}{\tau_{\mathrm{L}}^2 \tau_{\mathrm{R}}^2}\{\!\{\tau\}\!\}[\![\tau]\!] = 0, \quad \frac{3}{2}[\![\tau \mathcal{R}_{11}]\!] + \{\!\{u\}\!\}[\![u]\!] - \frac{g}{\tau_{\mathrm{L}}\tau_{\mathrm{R}}}[\![\tau]\!] = 0.$$

Using the first equation, we eliminate $[\![u]\!]$ from the second equation

$$\frac{3}{2}[\![\tau \mathcal{R}_{11}]\!] + \frac{\{\!\{u\}\!\}}{m}\left(\frac{g}{\tau_{\mathrm{L}}^2 \tau_{\mathrm{R}}^2}\{\!\{\tau\}\!\}[\![\tau]\!] - [\![\mathcal{R}_{11}]\!] \right) - \frac{g}{\tau_{\mathrm{L}}\tau_{\mathrm{R}}}[\![\tau]\!] = 0.$$

But since $\{\!\{u\}\!\}/m = \{\!\{\tau\}\!\}$, we get

$$\frac{3}{2}[\![\tau \mathcal{R}_{11}]\!] - \{\!\{\tau\}\!\}[\![\mathcal{R}_{11}]\!] + \frac{g}{\tau_{\mathrm{L}}\tau_{\mathrm{R}}}[\![\tau]\!]\left(\frac{\{\!\{\tau\}\!\}^2}{\tau_{\mathrm{L}}\tau_{\mathrm{R}}} - 1 \right) = 0$$

which upon simplification of the last term yields the Hugoniot curve (4.8). $\qquad \square$

We now find some constraints on the two states imposed by the Lax entropy condition if they have to be connected by a shock wave.

Theorem 4.9. *Any given admissible left and right states U_L, U_R can be connected by a*

- *1-shock wave if $h_R \in (h_L, 2h_L)$.*
- *6-shock wave if $h_L \in (h_R, 2h_R)$.*

Proof. Given the left state $(\tau_L, \mathcal{R}_{11}^L)$ the Hugoniot curve gives the set of right states $(\tau_R, \mathcal{R}_{11}^R)$ that can be connected to it by a shock. Using the Hugoniot curve, we can obtain the stress component at the right state as

$$\mathcal{R}_{11}^R = \frac{1}{2\tau_R - \tau_L}\left[(2\tau_L - \tau_R)\mathcal{R}_{11}^L - \frac{g[\![\tau]\!]^3}{2\tau_L^2\tau_R^2}\right] = R_{11}(\tau_R; \tau_L, \mathcal{R}_{11}^L)$$

where

$$\mathcal{R}_{11}(\tau; \tau_L, \mathcal{R}_{11}^L) = \frac{1}{2\tau - \tau_L}\left[(2\tau_L - \tau)\mathcal{R}_{11}^L - \frac{g(\tau - \tau_L)^3}{2\tau_L^2\tau^2}\right]. \tag{4.9}$$

When $\tau_R = \frac{1}{2}\tau_L$ we have $\mathcal{R}_{11}^R = \infty$ and moreover $\mathcal{R}_{11}^R < 0$ for $\tau_R < \frac{1}{2}\tau_L$. Hence from positivity requirement, the admissible range of values for τ_R is such that $\tau_R > \frac{1}{2}\tau_L$.

The Lax entropy condition says that characteristics must enter into the shock curve which means that, if S is the shock speed, we have

$$u_L - \sqrt{gh_L + 3\mathcal{P}_{11}^L} > S > u_R - \sqrt{gh_R + 3\mathcal{P}_{11}^R}$$

from which we obtain two Lax inequalities

$$u_L - S > \sqrt{gh_L + 3\mathcal{P}_{11}^L} > 0 \quad \text{and} \quad u_R - S < \sqrt{gh_R + 3\mathcal{P}_{11}^R}.$$

The first Lax inequality shows that the left state is the pre-shock state, since the velocity relative to the shock is positive. Using the jump condition of the continuity equation, $h_L(u_L - S) = h_R(u_R - S)$, we get

$$u_R - S > \frac{h_L}{h_R}\sqrt{gh_L + 3\mathcal{P}_{11}^L}.$$

Combining this with the second Lax inequality, we get

$$gh_L^3 + 3h_L\mathcal{R}_{11}^L < gh_R^3 + 3h_R\mathcal{R}_{11}^R \quad \Longrightarrow \quad \mathcal{R}_{11}^R > \mathcal{R}_{11}^\star(\tau_R; \tau_L, \mathcal{R}_{11}^L)$$

where the function $\mathcal{R}_{11}^\star(\tau; \tau_L, \mathcal{R}_{11}^L)$ is defined by

$$\mathcal{R}_{11}^\star(\tau; \tau_L, \mathcal{R}_{11}^L) = \frac{\tau}{3}\left[\frac{g}{\tau_L^3} - \frac{g}{\tau^3} + 3\frac{\mathcal{R}_{11}^L}{\tau_L}\right].$$

The entropy condition (second Lax inequality) requires that

$$\mathcal{R}_{11}^R = \mathcal{R}_{11}(\tau_R; \tau_L, \mathcal{R}_{11}^L) > \mathcal{R}_{11}^s(\tau_R; \tau_L, \mathcal{R}_{11}^L).$$

Now[1]

$$\frac{d}{d\tau}\mathcal{R}_{11}(\tau; \tau_L, \mathcal{R}_{11}^L) = -\frac{g(\tau - \tau_L)^2(4\tau - \tau_L) + 6\tau_L^4\mathcal{R}_{11}^L}{2\tau_L^3(2\tau - \tau_L)^2} < 0, \quad \tau > \frac{1}{2}\tau_L$$

and

$$\frac{d}{d\tau}\mathcal{R}_{11}^\star(\tau; \tau_L, \mathcal{R}_{11}^L) = \frac{g}{3}\left(\frac{2}{\tau^3} + \frac{1}{\tau_L^3}\right) + \frac{\mathcal{R}_{11}^L}{\tau_L} > 0, \quad \tau > 0.$$

---

[1]We are not interested in the case $\tau \le \frac{1}{2}\tau_L$.

This shows that for $\tau > \frac{1}{2}\tau_{\mathrm{L}}$, $\mathcal{R}_{11}(\tau; \tau_{\mathrm{L}}, \mathcal{R}_{11}^{\mathrm{L}})$ is a decreasing function and $\mathcal{R}_{11}^{\star}(\tau; \tau_{\mathrm{L}}, \mathcal{R}_{11}^{\mathrm{L}})$ is an increasing function; moreover $\mathcal{R}_{11}(\frac{1}{2}\tau_{\mathrm{L}}; \tau_{\mathrm{L}}, \mathcal{R}_{11}^{\mathrm{L}}) = \infty > \mathcal{R}_{11}^{\star}(\frac{1}{2}\tau_{\mathrm{L}}; \tau_{\mathrm{L}}, \mathcal{R}_{11}^{\mathrm{L}})$ and $\mathcal{R}_{11}(\tau_{\mathrm{L}}; \tau_{\mathrm{L}}, \mathcal{R}_{11}^{\mathrm{L}}) = \mathcal{R}_{11}^{\star}(\tau_{\mathrm{L}}; \tau_{\mathrm{L}}, \mathcal{R}_{11}^{\mathrm{L}})$. Hence

$$\mathcal{R}_{11}(\tau; \tau_{\mathrm{L}}, \mathcal{R}_{11}^{\mathrm{L}}) > \mathcal{R}_{11}^{\star}(\tau; \tau_{\mathrm{L}}, \mathcal{R}_{11}^{\mathrm{L}}), \quad \text{if and only if } \tau \in \left(\frac{1}{2}\tau_{\mathrm{L}}, \tau_{\mathrm{L}}\right).$$

The admissible range of values for τ_{R} is $\left(\frac{1}{2}\tau_{\mathrm{L}}, \tau_{\mathrm{L}}\right)$ and hence $h_{\mathrm{R}} \in (h_{\mathrm{L}}, 2h_{\mathrm{L}})$. Across a shock wave, the water depth h can at most increase by a factor of less than two.

The proof for the 6-shock case follows similarly.   □

Lemma 4.10. (1) *If the left and right states $\boldsymbol{U}_{\mathrm{L}}, \boldsymbol{U}_{\mathrm{R}}$ are connected by a 1-shock, then: $u_{\mathrm{R}} < u_{\mathrm{L}}$ and $\mathrm{P}_{\mathrm{R}} > \mathrm{P}_{\mathrm{L}}$.*
(2) *If the left and right states $\boldsymbol{U}_{\mathrm{L}}, \boldsymbol{U}_{\mathrm{R}}$ are connected by a 6-shock, then: $u_{\mathrm{L}} > u_{\mathrm{R}}$ and $\mathrm{P}_{\mathrm{L}} > \mathrm{P}_{\mathrm{R}}$.*
(3) *Moreover, in either case, we have*

$$u_{\mathrm{L}} - u_{\mathrm{R}} = \sqrt{\frac{(h_{\mathrm{R}} - h_{\mathrm{L}})(\mathrm{P}_{\mathrm{R}} - \mathrm{P}_{\mathrm{L}})}{h_{\mathrm{R}} h_{\mathrm{L}}}}. \tag{4.10}$$

Proof. (1) The jump condition of the continuity equation, $h_{\mathrm{L}}(u_{\mathrm{L}} - S) = h_{\mathrm{R}}(u_{\mathrm{R}} - S)$, when applied to the 1-wave, gives

$$u_{\mathrm{R}} = \underbrace{\frac{h_{\mathrm{L}}}{h_{\mathrm{R}}}}_{\in(\frac{1}{2},1)} \underbrace{(u_{\mathrm{L}} - S)}_{>0} + S \leq u_{\mathrm{L}} - S + S = u_{\mathrm{L}}.$$

Thus the post-shock velocity u_{R} is smaller than the pre-shock velocity u_{L}. The total pressure is defined as $\mathrm{P} = \mathcal{R}_{11} + \frac{1}{2}gh^2$. Then, using the Hugoniot curve, we have

$$\mathrm{P}_{\mathrm{R}} - \mathrm{P}_{\mathrm{L}} = \frac{3(h_{\mathrm{R}} - h_{\mathrm{L}})}{2h_{\mathrm{L}} - h_{\mathrm{R}}}\mathcal{R}_{11}^{\mathrm{L}} + \frac{1}{2}g\frac{h_{\mathrm{L}}(h_{\mathrm{R}}^2 - 4h_{\mathrm{R}}h_{\mathrm{L}} + 3h_{\mathrm{L}}^2)}{h_{\mathrm{R}} - 2h_{\mathrm{L}}}$$

and since $h_{\mathrm{R}} \in (h_{\mathrm{L}}, 2h_{\mathrm{L}})$, both terms on the right of the above equation are positive, so that $\mathrm{P}_{\mathrm{R}} > \mathrm{P}_{\mathrm{L}}$.

(2) In the context of a 6-shock, we have

$$u_{\mathrm{L}} = \underbrace{\frac{h_{\mathrm{R}}}{h_{\mathrm{L}}}}_{\in(\frac{1}{2},1)} \underbrace{(u_{\mathrm{R}} - S)}_{<0} + S \geq u_{\mathrm{R}} - S + S = u_{\mathrm{R}}.$$

In this context, "R" is pre-shock state and "L" is post-shock state. Similarly as for the 1-wave, we obtain that $u_{\mathrm{L}} < u_{\mathrm{R}}$ and $\mathrm{P}_{\mathrm{R}} > \mathrm{P}_{\mathrm{L}}$.

(3) Dividing the jump conditions for continuity and x-momentum equations, we get

$$\left(\mathrm{P}_{\mathrm{R}} + h_{\mathrm{R}}u_{\mathrm{R}}^2 - \mathrm{P}_{\mathrm{L}} - h_{\mathrm{L}}u_{\mathrm{L}}^2\right)(h_{\mathrm{R}} - h_{\mathrm{L}}) = h_{\mathrm{R}}^2 u_{\mathrm{R}}^2 + h_{\mathrm{L}}^2 u_{\mathrm{L}}^2 - 2h_{\mathrm{L}}h_{\mathrm{R}}u_{\mathrm{L}}u_{\mathrm{R}}.$$

Simplifying we obtain a quadratic equation

$$u_{\mathrm{R}}^2 - 2u_{\mathrm{L}}u_{\mathrm{R}} + u_{\mathrm{L}}^2 - \frac{(h_{\mathrm{R}} - h_{\mathrm{L}})(\mathrm{P}_{\mathrm{R}} - \mathrm{P}_{\mathrm{L}})}{h_{\mathrm{R}} h_{\mathrm{L}}} = 0$$

whose solution is

$$u_{\mathrm{R}} = u_{\mathrm{L}} \pm \sqrt{\frac{(h_{\mathrm{R}} - h_{\mathrm{L}})(\mathrm{P}_{\mathrm{R}} - \mathrm{P}_{\mathrm{L}})}{h_{\mathrm{R}} h_{\mathrm{L}}}}.$$

If we pick the minus sign, then we satisfy the conditions in part (1) and (2) of the lemma which yields (4.10).
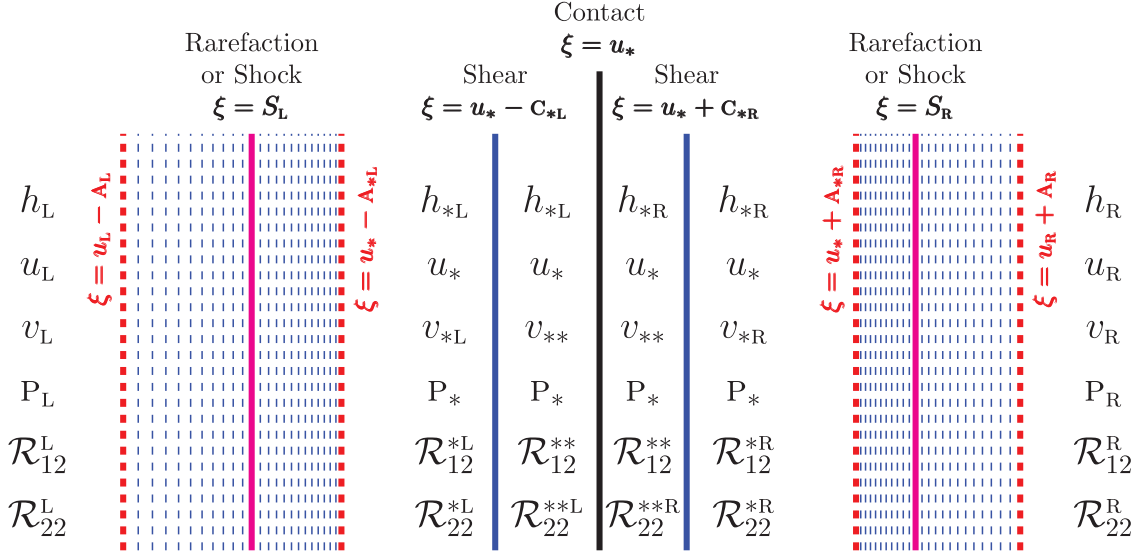   □

FIGURE 2. Shear Shallow Water (SSW) model: Wave structure of the 1-D Riemann problem. Usefull set of variables in the intermediate states for the computation of the analytical solution.

5. EXACT SOLUTION OF 1-D RIEMANN PROBLEM

The Riemann problem is an initial value problem where the initial data is discontinuous at a single point. The Riemann problem is to find $\boldsymbol{U}(t,x)$ solution of the SSW system (2.6), with the following initial data

$$\boldsymbol{U}(t=0,x) = \begin{cases} \boldsymbol{U}_{\mathrm{L}} & \text{if } x < 0 \\ \boldsymbol{U}_{\mathrm{R}} & \text{if } x > 0. \end{cases} \tag{5.1}$$

Lemma 5.1. *The solution of the Riemann problem with states $\boldsymbol{U}_{\mathrm{L}}, \boldsymbol{U}_{\mathrm{R}}$ gives rise to four intermediate states denoted by $\boldsymbol{U}_{*\mathrm{L}}, \boldsymbol{U}_{**\mathrm{L}}, \boldsymbol{U}_{**\mathrm{R}}, \boldsymbol{U}_{*\mathrm{R}}$ which satisfy the following ten relations, see Figure 2.*

$$u_{*\mathrm{L}} = u_{**\mathrm{L}} = u_{**\mathrm{R}} = u_{*\mathrm{R}}, \quad \mathrm{P}_{*\mathrm{L}} = \mathrm{P}_{**\mathrm{L}} = \mathrm{P}_{**\mathrm{R}} = \mathrm{P}_{*\mathrm{R}}$$
$$h_{*\mathrm{L}} = h_{**\mathrm{L}}, \quad h_{**\mathrm{R}} = h_{*\mathrm{R}}, \quad v_{**\mathrm{L}} = v_{**\mathrm{R}}, \quad \mathcal{R}_{12}^{**\mathrm{L}} = \mathcal{R}_{12}^{**\mathrm{R}}.$$

Using the definition of the total pressure, a consequence the previous relations is that $\mathcal{R}_{11}^{*\mathrm{L}} = \mathcal{R}_{11}^{**\mathrm{L}}$ and $\mathcal{R}_{11}^{**\mathrm{R}} = \mathcal{R}_{11}^{*\mathrm{R}}$.

The solution is obtained by using the constancy of total pressure (P_*) and normal velocity (u_*) inside the Riemann fan. If the 1-wave is a rarefaction, then $h_{*\mathrm{L}} \leq h_{\mathrm{L}}$ while if it is a shock, then $h_{*\mathrm{L}} \in (h_{\mathrm{L}}, 2h_{\mathrm{L}})$. Similarly, if the 6-wave is a rarefaction then $h_{*\mathrm{R}} < h_{\mathrm{R}}$, while if it is a shock, then $h_{*\mathrm{R}} \in (h_{\mathrm{R}}, 2h_{\mathrm{R}})$. The total pressure in the first intermediate state can be written as

$$\mathrm{P}_{*\mathrm{L}} = \begin{cases} \left(\frac{h_{*\mathrm{L}}}{h_{\mathrm{L}}}\right)^3 \mathcal{R}_{11}^{\mathrm{L}} + \frac{1}{2}gh_{*\mathrm{L}}^2 & \text{for a 1-rarefaction} : h_{*\mathrm{L}} \leq h_{\mathrm{L}} \\ \frac{1}{2h_{\mathrm{L}}-h_{*\mathrm{L}}}\left[(2h_{*\mathrm{L}} - h_{\mathrm{L}})\mathcal{R}_{11}^{\mathrm{L}} - \frac{g(h_{\mathrm{L}}-h_{*\mathrm{L}})^3}{2}\right] + \frac{1}{2}gh_{*\mathrm{L}}^2 & \text{for a 1-shock} : h_{*\mathrm{L}} > h_{\mathrm{L}}. \end{cases} \tag{5.2}$$

The velocity is given by

$$u_{*\mathrm{L}} = \begin{cases} u_{\mathrm{L}} - \left[\mathfrak{a}(h_{*\mathrm{L}}, c_{\mathrm{L}}) - \mathfrak{a}(h_{\mathrm{L}}, c_{\mathrm{L}})\right] & \text{for a 1-rarefaction} : h_{*\mathrm{L}} \leq h_{\mathrm{L}} \\ u_{\mathrm{L}} - \sqrt{\frac{(h_{*\mathrm{L}} - h_{\mathrm{L}})(P_{*\mathrm{L}} - P_{\mathrm{L}})}{h_{*\mathrm{L}} h_{\mathrm{L}}}} & \text{for a 1-shock} : h_{*\mathrm{L}} > h_{\mathrm{L}}. \end{cases}$$

For the 6-wave, and given right state, we have

$$P_{*\mathrm{R}} = \begin{cases} \left(\frac{h_{*\mathrm{L}}}{h_{\mathrm{R}}}\right)^3 \mathcal{R}_{11}^{\mathrm{R}} + \frac{1}{2} g h_{*\mathrm{R}}^2 & \text{for a 6-rarefaction} : h_{*\mathrm{R}} \leq h_{\mathrm{R}} \\ \frac{1}{2h_{\mathrm{R}} - h_{*\mathrm{R}}}\left[(2h_{*\mathrm{R}} - h_{\mathrm{R}})\mathcal{R}_{11}^{\mathrm{R}} - \frac{g(h_{\mathrm{R}} - h_{*\mathrm{R}})^3}{2}\right] + \frac{1}{2} g h_{*\mathrm{R}}^2 & \text{for a 6-shock} : h_{*\mathrm{R}} > h_{\mathrm{R}} \end{cases}$$

and

$$u_{*\mathrm{R}} = \begin{cases} u_{\mathrm{R}} + \left[\mathfrak{a}(h_{*\mathrm{R}}, c_{\mathrm{R}}) - \mathfrak{a}(h_{\mathrm{R}}, c_{\mathrm{R}})\right] & \text{for a 6-rarefaction} : h_{*\mathrm{R}} \leq h_{\mathrm{R}} \\ u_{\mathrm{R}} + \sqrt{\frac{(h_{*\mathrm{R}} - h_{\mathrm{R}})(P_{*\mathrm{R}} - P_{\mathrm{R}})}{h_{*\mathrm{R}} h_{\mathrm{R}}}} & \text{for a 6-shock} : h_{*\mathrm{R}} > h_{\mathrm{R}}. \end{cases}$$

We now want to determine $z_{\mathrm{L}} = \frac{h_{*\mathrm{L}}}{h_{\mathrm{L}}}$ and $z_{\mathrm{R}} = \frac{h_{*\mathrm{R}}}{h_{\mathrm{R}}}$ such that the total pressure and the velocity obtained from the 1-wave matches with those obtained from the 6-wave:

$$P_{*\mathrm{L}} - P_{*\mathrm{R}} = 0 \quad \text{and} \quad u_{*\mathrm{L}} - u_{*\mathrm{R}} = 0.$$

We define the functions $f(z; h, \mathcal{R}_{11})$ for the total pressure and $g_{\pm}(z; h, u, \mathcal{R}_{11})$ for the velocity as

$$f(z; h, \mathcal{R}_{11}) = \begin{cases} z^3 \mathcal{R}_{11} + \frac{1}{2} g z^2 h^2 & 0 < z \leq 1 \\ \frac{2z-1}{2-z} \mathcal{R}_{11} + \frac{1}{2} g h^2 \frac{(z-1)^3}{2-z} + \frac{1}{2} g z^2 h^2 & 1 < z < 2 \end{cases}$$

and

$$g_{\pm}(z; h, u, \mathcal{R}_{11}) = \begin{cases} u \pm [\mathfrak{a}(zh, c) - \mathfrak{a}(h, c)] & 0 < z \leq 1 \\ u \pm \sqrt{\frac{(z-1)[f(z; h, \mathcal{R}_{11}) - \mathcal{R}_{11} - \frac{1}{2} g h^2]}{zh}} & 1 < z < 2 \end{cases}$$

where $c = \mathcal{R}_{11}/h^3$. The problem can now be stated as:

$$\text{find} \quad z_{\mathrm{L}}, z_{\mathrm{R}} \in (0, 2) \quad \text{such that} \quad \begin{cases} F(z_{\mathrm{L}}, z_{\mathrm{R}}) = 0 \\ G(z_{\mathrm{L}}, z_{\mathrm{R}}) = 0 \end{cases} \tag{5.3}$$

where

$$\begin{aligned} F(z_1, z_2) &= f(z_1; h_{\mathrm{L}}, \mathcal{R}_{11}^{\mathrm{L}}) - f(z_2; h_{\mathrm{R}}, \mathcal{R}_{11}^{\mathrm{R}}) \\ G(z_1, z_2) &= g_{-}(z_1; h_{\mathrm{L}}, u_{\mathrm{L}}, \mathcal{R}_{11}^{\mathrm{L}}) - g_{+}(z_2; h_{\mathrm{R}}, u_{\mathrm{R}}, \mathcal{R}_{11}^{\mathrm{R}}). \end{aligned} \tag{5.4}$$

If the solution is such that $z_{\mathrm{L}} \in (0, 1)$ then the 1-wave is a rarefaction, and otherwise if $z_{\mathrm{L}} \in (1, 2)$, then it is a 1-shock. Similar interpretation applies to the 6-wave. The roots can be obtained by a Newton method as described in Appendix A.

We can numerically investigate the above functions F, G by plotting contours of their level sets. For a given Riemann data of dam break problem from Section 7.1, we plot contours of F, G and also plot their zero contour lines. The solution is at the intersection of the zero contour lines of the two functions. In the Figure 3, the bold solid lines are the zero level curves of F, G and we see that they intersect at a unique point, which is approximately

$$z_{\mathrm{L}} = 0.731428410320821, \quad z_{\mathrm{R}} = 1.4177231168358784.$$

Hence the 1-wave is a 1-rarefaction and the 6-wave is a 6-shock. We observe that the level curves of F, G have a monotonic behaviour which implies that they intersect at a unique point and we now prove this behaviour in the general case.
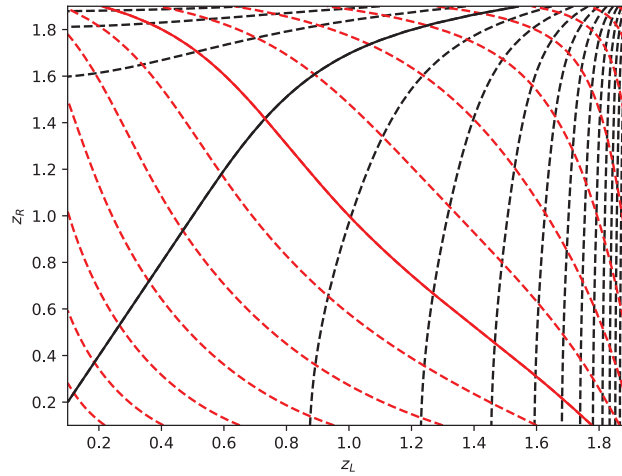
FIGURE 3. Contours of F (black) and G (red) for dam break problem. Solid lines are where the functions are zero. Intersection of the solid lines gives the desired z_{L} and z_{R}.

Theorem 5.2. *Assume that the two states in the Riemann problem are positive $(h_{\mathrm{L}}, h_{\mathrm{R}} > 0)$. If*

$$u_{\mathrm{R}} - u_{\mathrm{L}} < \mathfrak{a}(h_{\mathrm{L}}, c_{\mathrm{L}}) + \mathfrak{a}(h_{\mathrm{R}}, c_{\mathrm{R}}) \tag{5.5}$$

where $\mathfrak{a}(h, c)$ is given by (4.3), then there exists a unique solution $(z_{\mathrm{L}}, z_{\mathrm{R}}) \in (0, 2) \times (0, 2)$ such that

$$F(z_{\mathrm{L}}, z_{\mathrm{R}}) = 0 \quad \text{and} \quad G(z_{\mathrm{L}}, z_{\mathrm{R}}) = 0 \tag{5.6}$$

where F, G are given by (5.4). In this context, the Riemann problem has a unique, positive solution.

Proof. We want to show that the set of equations (5.6) has a unique solution $(z_{\mathrm{L}}, z_{\mathrm{R}}) \in (0, 2) \times (0, 2)$. Now

$$\frac{\partial F}{\partial z_{\mathrm{L}}} = \frac{\partial}{\partial z_{\mathrm{L}}} f(z_{\mathrm{L}}; h_{\mathrm{L}}, \mathcal{R}_{11}^{\mathrm{L}}) = \begin{cases} 3z_{\mathrm{L}}^2 \mathcal{R}_{11}^{\mathrm{L}} + g z_{\mathrm{L}} h_{\mathrm{L}}^2, & 0 < z_{\mathrm{L}} \leq 1 \\ \frac{3}{(2-z_{\mathrm{L}})^2} \mathcal{R}_{11}^{\mathrm{L}} + \frac{1}{2} g h_{\mathrm{L}}^2 \frac{z_{\mathrm{L}}^2 - 4z_{\mathrm{L}} + 5}{(2-z_{\mathrm{L}})^2}, & 1 \leq z_{\mathrm{L}} < 2. \end{cases}$$

Hence $f(z; h, \mathcal{R}_{11})$ is an increasing function of $z \in (0, 2)$ with $f(0; h, \mathcal{R}_{11}) = 0$ and $f(2; h, \mathcal{R}_{11}) = \infty$. Thus given any $z_{\mathrm{L}} \in (0, 2)$, the equation $F(z_{\mathrm{L}}, z_{\mathrm{R}}) = 0$ has a unique solution $z_{\mathrm{R}} \in (0, 2)$ Now, since

$$\frac{\partial F}{\partial z_{\mathrm{L}}} > 0, \quad \frac{\partial F}{\partial z_{\mathrm{R}}} < 0, \quad z_{\mathrm{L}}, z_{\mathrm{R}} \in (0, 2)$$

then by implicit function theorem, we have a continuously differentiable function $z_{\mathrm{R}} = \hat{z}_{\mathrm{R}}(z_{\mathrm{L}})$, $z_{\mathrm{L}} \in (0, 2)$ such that $F(z_{\mathrm{L}}, \hat{z}_{\mathrm{R}}(z_{\mathrm{L}})) = 0$. Moreover $F(0, 0) = 0$ so that $\hat{z}_{\mathrm{R}}(0) = 0$. Now

$$\frac{\mathrm{d}\hat{z}_{\mathrm{R}}}{\mathrm{d}z_{\mathrm{L}}} = -\frac{\frac{\partial F}{\partial z_{\mathrm{L}}}}{\frac{\partial F}{\partial z_{\mathrm{R}}}} > 0, \quad z_{\mathrm{L}} \in (0, 2)$$

so that $\hat{z}_{\mathrm{R}}(z_{\mathrm{L}})$ is an increasing function. Now

$$\frac{\mathrm{d}\hat{z}_{\mathrm{R}}}{\mathrm{d}z_{\mathrm{L}}}(0) = \lim_{z_{\mathrm{L}} \to 0} \frac{3z_{\mathrm{L}}^2 \mathcal{R}_{11}^{\mathrm{L}} + g z_{\mathrm{L}} h_{\mathrm{L}}^2}{3\hat{z}_{\mathrm{R}}(z_{\mathrm{L}})^2 \mathcal{R}_{11}^{\mathrm{R}} + g \hat{z}_{\mathrm{R}}(z_{\mathrm{L}}) h_{\mathrm{R}}^2}$$

which is of $0/0$ form. Applying L'Hopital rule, we get

$$\frac{\mathrm{d}\hat{z}_{\mathrm{R}}}{\mathrm{d}z_{\mathrm{L}}}(0) = \lim_{z_{\mathrm{L}}\to 0} \frac{6z_{\mathrm{L}}\mathcal{R}_{11}^{\mathrm{L}} + gh_{\mathrm{L}}^2}{6\hat{z}_{\mathrm{R}}(z_{\mathrm{L}})\frac{\mathrm{d}\hat{z}_{\mathrm{R}}}{\mathrm{d}z_{\mathrm{L}}}(z_{\mathrm{L}})\mathcal{R}_{11}^{\mathrm{R}} + g\frac{\mathrm{d}\hat{z}_{\mathrm{R}}}{\mathrm{d}z_{\mathrm{L}}}(z_{\mathrm{L}})h_{\mathrm{R}}^2} = \frac{h_{\mathrm{L}}^2}{\frac{\mathrm{d}\hat{z}_{\mathrm{R}}}{\mathrm{d}z_{\mathrm{L}}}(0)h_{\mathrm{R}}^2} \quad \Longrightarrow \quad \frac{\mathrm{d}\hat{z}_{\mathrm{R}}}{\mathrm{d}z_{\mathrm{L}}}(0) = \frac{h_{\mathrm{L}}}{h_{\mathrm{R}}} > 0.$$

As $z_{\mathrm{L}} \to 2$, the first term of F in (5.4) which depends on z_{L} goes to ∞ and this requires that $z_{\mathrm{R}} \to 2$ also, *i.e.*, $\hat{z}_{\mathrm{R}}(z_{\mathrm{L}}) \to 2$. Moreover, $\hat{z}_{\mathrm{R}}(z_{\mathrm{L}}) \neq 2$ for $z_{\mathrm{L}} \in (0,2)$ since the second term in F goes to ∞ as $z_{\mathrm{R}} \to 2$. Hence the curve $(z_{\mathrm{L}}, \hat{z}_{\mathrm{R}}(z_{\mathrm{L}}))$ starts at $(0,0)$ and approaches $(2,2)$ in a monotonic way.

Now consider the function G for which

$$\frac{\partial G}{\partial z_{\mathrm{L}}} = \frac{\partial}{\partial z_{\mathrm{L}}} g_-(z_{\mathrm{L}}; h_{\mathrm{L}}, u_{\mathrm{L}}, \mathcal{R}_{11}^{\mathrm{L}}) = \begin{cases} -\frac{1}{z_{\mathrm{L}}}\sqrt{gh_{\mathrm{L}}z_{\mathrm{L}} + 3z_{\mathrm{L}}^2\mathcal{R}_{11}^{\mathrm{L}}/h_{\mathrm{L}}} & 0 < z_{\mathrm{L}} \leq 1 \\[2mm] -\frac{6\mathcal{R}_{11}^{\mathrm{L}} + \frac{1}{2}gh_{\mathrm{L}}^2\left(z_{\mathrm{L}}^3 - 3z_{\mathrm{L}}+6\right)}{2[z_{\mathrm{L}}(2-z_{\mathrm{L}})]^{3/2}h_{\mathrm{L}}^{1/2}\left[3\mathcal{R}_{11}^{\mathrm{L}} + \frac{1}{2}gh_{\mathrm{L}}^2(3-z_{\mathrm{L}})\right]^{1/2}} & 1 \leq z_{\mathrm{L}} < 2 \end{cases}$$

with a similar expression for $\frac{\partial G}{\partial z_{\mathrm{R}}}$. Hence

$$\frac{\partial G}{\partial z_{\mathrm{L}}} < 0, \quad \frac{\partial G}{\partial z_{\mathrm{R}}} < 0, \quad z_{\mathrm{L}}, z_{\mathrm{R}} \in (0,2).$$

Thus $g_-(z; h, u, \mathcal{R}_{11})$ is a decreasing function and $g_+(z; h, u, \mathcal{R}_{11})$ is an increasing function in $(0,2)$, see Figure 4, and moreover

$$g_-(0; h_{\mathrm{L}}, u_{\mathrm{L}}, \mathcal{R}_{11}^{\mathrm{L}}) = u_{\mathrm{L}} + \mathfrak{a}(h_{\mathrm{L}}, c_{\mathrm{L}}), \quad g_-(2; h_{\mathrm{L}}, u_{\mathrm{L}}, \mathcal{R}_{11}^{\mathrm{L}}) = -\infty$$
$$g_+(0; h_{\mathrm{R}}, u_{\mathrm{R}}, \mathcal{R}_{11}^{\mathrm{R}}) = u_{\mathrm{R}} - \mathfrak{a}(h_{\mathrm{R}}, c_{\mathrm{R}}), \quad g_+(2; h_{\mathrm{R}}, u_{\mathrm{R}}, \mathcal{R}_{11}^{\mathrm{R}}) = +\infty.$$

Under the assumption (5.5), we have $g_-(0; h_{\mathrm{L}}, u_{\mathrm{L}}, \mathcal{R}_{11}^{\mathrm{L}}) > g_+(0; h_{\mathrm{R}}, u_{\mathrm{R}}, \mathcal{R}_{11}^{\mathrm{R}})$, and the equation $G(z_{\mathrm{L}}, z_{\mathrm{R}}) = 0$ has a unique solution $z_{\mathrm{R}} = \tilde{z}_{\mathrm{R}}(z_{\mathrm{L}}) \in [0,2)$ for all $z_{\mathrm{L}} \in [0, z_{\mathrm{L}}^*]$ with $\tilde{z}_{\mathrm{R}}(z_{\mathrm{L}}^*) = 0$ where z_{L}^* satisfies $g_-(z_{\mathrm{L}}^*; h_{\mathrm{L}}, u_{\mathrm{L}}, \mathcal{R}_{11}^{\mathrm{L}}) = g_+(0; h_{\mathrm{R}}, u_{\mathrm{R}}, \mathcal{R}_{11}^{\mathrm{R}}) = u_{\mathrm{R}} - \mathfrak{a}(h_{\mathrm{R}}, c_{\mathrm{R}})$. By implicit function theorem, there is a continuously differentiable function $z_{\mathrm{R}} = \tilde{z}_{\mathrm{R}}(z_{\mathrm{L}})$, $z_{\mathrm{L}} \in [0, z_{\mathrm{L}}^*]$ such that $G(z_{\mathrm{L}}, \tilde{z}_{\mathrm{R}}(z_{\mathrm{L}})) = 0$. Now

$$\frac{\mathrm{d}\tilde{z}_{\mathrm{R}}}{\mathrm{d}z_{\mathrm{L}}} = -\frac{\frac{\partial G}{\partial z_{\mathrm{L}}}}{\frac{\partial G}{\partial z_{\mathrm{R}}}} < 0, \quad z_{\mathrm{L}} \in [0, z_{\mathrm{L}}^*]$$

so that $\tilde{z}_{\mathrm{R}}(z_{\mathrm{L}})$ is a decreasing function for $z_{\mathrm{L}} \in [0, z_{\mathrm{L}}^*]$.

We have shown that $\hat{z}_{\mathrm{R}} : [0,2) \to [0,2)$ is increasing function with $\hat{z}_{\mathrm{R}}(0) = 0$, $\lim_{z_{\mathrm{L}}\to 2} \hat{z}_{\mathrm{R}}(z_{\mathrm{L}}) = 2$, and $\tilde{z}_{\mathrm{R}} : [0, z_{\mathrm{L}}^*] \to [0,2)$ is decreasing function with $\tilde{z}_{\mathrm{R}}(0) \in (0,2)$, $\tilde{z}_{\mathrm{R}}(z_{\mathrm{L}}^*) = 0$, so they intersect at a unique point in $z_{\mathrm{L}} \in (0,2)$ which is the desired solution. $\qquad\square$

5.1. Shock speed and jump conditions

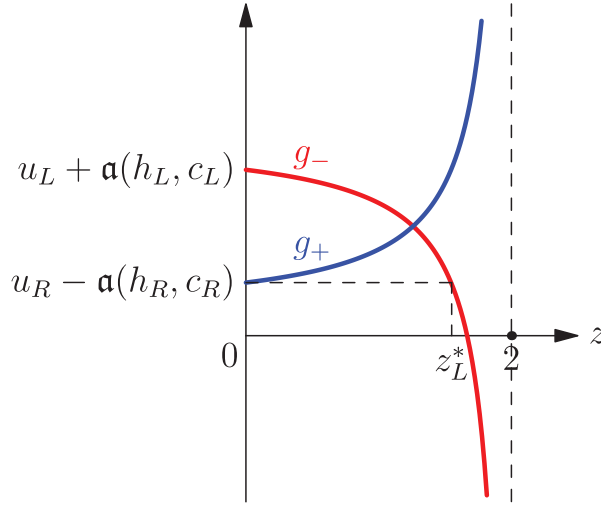Suppose that the 1-wave is a 1-shock; then $h_{*\mathrm{L}} = z_{\mathrm{L}}h_{\mathrm{L}}$ and using (4.9)

$$\mathcal{R}_{11}^{*\mathrm{L}} = \mathcal{R}_{11}(z_{\mathrm{L}}h_{\mathrm{L}}; h_{\mathrm{L}}, \mathcal{R}_{11}^{\mathrm{L}}) = \frac{2z_{\mathrm{L}} - 1}{2 - z_{\mathrm{L}}}\mathcal{R}_{11}^{\mathrm{L}} + \frac{1}{2}gh_{\mathrm{L}}^2\frac{(z_{\mathrm{L}}-1)^3}{2 - z_{\mathrm{L}}} \tag{5.7}$$

while (4.10) yields

$$u_* = u_{*\mathrm{L}} = u_{\mathrm{L}} - \sqrt{\frac{(h_{*\mathrm{L}} - h_{\mathrm{L}})(\mathrm{P}_{*\mathrm{L}} - \mathrm{P}_{\mathrm{L}})}{h_{*\mathrm{L}}h_{\mathrm{L}}}}. \tag{5.8}$$

The 1-shock speed can be computed from the jump condition (3.3a)

$$S_{\mathrm{L}} = \frac{[\![hu]\!]}{[\![h]\!]} = \{\!\{u\}\!\} + \{\!\{h\}\!\}\frac{[\![u]\!]}{[\![h]\!]} = \frac{u_{\mathrm{L}} + u_*}{2} + \left(\frac{z_{\mathrm{L}} + 1}{z_{\mathrm{L}} - 1}\right)\frac{u_* - u_{\mathrm{L}}}{2}. \tag{5.9}$$

FIGURE 4. Illustration of the functions $g_\pm$ under the condition (5.5).

The jump conditions (3.3a), (3.3b), (3.3d) have already been satisfied since they were used to determine the Hugoniot curve. We can find $v_{*L}, \mathcal{R}_{12}^{*L}$ from (3.3c), (3.3e) which is a linear system of equations

$$\begin{cases} h_{*L}(u_* - S_L)v_{*L} + \mathcal{R}_{12}^{*L} = a_1 \\ \left(\frac{1}{2}\mathcal{R}_{11}^{*L} + \frac{1}{2}h_{*L}u_*(u_* - S_L) + \frac{1}{4}gh_{*L}(h_{*L} - h_L)\right)v_{*L} + \left(u_* - \frac{1}{2}S_L\right)\mathcal{R}_{12}^{*L} = a_2 \end{cases} \tag{5.10}$$

where

$$a_1 = h_L(u_L - S_L)v_L + \mathcal{R}_{12}^L$$
$$a_2 = (u_L - S_L)\mathcal{E}_{12}^L + \frac{1}{2}(\mathcal{R}_{11}^L v_L + \mathcal{R}_{12}^L u_L) - \frac{1}{4}gh_L v_L(h_{*L} - h_L).$$

The determinant of the 2×2 matrix is

$$Det = -\frac{1}{2}\mathcal{R}_{11}^{*L} + \frac{1}{2}h_{*L}(u_* - S_L)^2 - \frac{1}{4}gh_{*L}(h_{*L} - h_L).$$

But using (5.9) and (5.8)

$$u_* - S_L = -\frac{u_* - u_L}{z_L - 1} = \sqrt{\frac{(P_{*L} - P_L)}{(z_L - 1)h_{*L}}}$$

and hence, using (5.7), we get

$$Det = \frac{2 - z_L}{2(z_L - 1)}\mathcal{R}_{11}^{*L} - \frac{\mathcal{R}_{11}^L}{2(z_L - 1)} + \frac{1}{4}gh_L^2(1 + 2z_L - z_L^2) = R_{11}^L + \frac{1}{2}gh_L^2 = P_L > 0$$

and hence the 2×2 system has a unique solution. Once $v_{*L}, \mathcal{R}_{12}^{*L}$ have been determined, we can compute $\mathcal{R}_{22}^{*L}$ from (3.3f)

$$\mathcal{E}_{22}^{*L} = \frac{1}{u_* - S_L}[(u_L - S_L)\mathcal{E}_{22}^L - (\mathcal{R}_{12}^{*L}v_{*L} - \mathcal{R}_{12}^L v_L)], \quad \mathcal{R}_{22}^{*L} = 2\mathcal{E}_{22}^{*L} - h_{*L}v_{*L}^2.$$

We have thus satisfied all the jump conditions and completely determined the $\boldsymbol{U}_{*L}$ state. The jump conditions for a 6-shock can be satisfied in a similar way to determine the $\boldsymbol{U}_{*R}$ state.

Shock speed. If the 1-wave is a shock, then $1 < z_L < 2$ and from (5.2)

$$P_{*L} - P_L = \frac{z_L - 1}{2 - z_L}\left[3\mathcal{R}_{11}^L + \frac{1}{2}gh_L^2(3 - z_L)\right] \tag{5.11}$$

and the shock speed is given by

$$\begin{aligned} S_L &= \frac{z_L u_* - u_L}{z_L - 1} \quad \text{from (5.9)} \\ &= u_L - \sqrt{\frac{z_L}{2 - z_L}\left[3\mathcal{P}_{11}^L + \frac{1}{2}gh_L(3 - z_L)\right]}, \quad \text{from (5.8) and (5.11).} \end{aligned} \tag{5.12}$$

Similarly, the speed of the 6-shock is given by

$$S_R = u_R + \sqrt{\frac{z_R}{2 - z_R}\left[3\mathcal{P}_{11}^R + \frac{1}{2}gh_R(3 - z_R)\right]}.$$

Remark 5.3. In HLL-type solvers, it is necessary to have estimates of the slowest and fastest speeds arising in the solution of the Riemann problem. If the 1-wave is a shock, then we would like a lower bound $\tilde{S}_L$ on this speed

$$S_L \geq \tilde{S}_L := u_L - \sup_{z \in (1,2)} \sqrt{\frac{z}{2 - z}\left[3\mathcal{P}_{11}^L + \frac{1}{2}gh_L(3 - z)\right]}.$$

But the supremum is ∞ and we do not get a useful lower bound.

5.2. Resumed computation of the intermediate states.

For a Riemann problem, the left (U_L) and the right (U_R) states are input data.

– For given U_L and U_R, the system (5.3) is solved and z_L, z_R are obtained. Therefore,

$$\begin{aligned} h_{*L} &= z_L h_L, & u_* &= g_-(z_L; h_L, u_L, \mathcal{R}_{11}^L) = g_+(z_R; h_R, u_R, \mathcal{R}_{11}^R), \\ h_{*R} &= z_R h_R, & P_* &= f(z_L; h_L, \mathcal{R}_{11}^L) & = f(z_R; h_R, \mathcal{R}_{11}^R). \end{aligned}$$

The variables h and P are now defined for all intermediate states. Using the definition of the total pressure $P = \frac{gh^2}{2} + \mathcal{R}_{11}$, we can get $\mathcal{R}_{11}^{*L}$ and $\mathcal{R}_{11}^{*R}$.

– When $z_L \leq 1$ the 1-wave is a rarefaction. The associated Riemann invariants are used to compute v_{*L}, $\mathcal{R}_{12}^{*L}$ and $\mathcal{R}_{12}^{*L}$. The internal structure of the rarefaction is obtained by integration of equations for the 1-wave integral curve. Similarly, when $z_R \leq 1$, Riemann invariants for 6-rarefaction are used to compute v_{*R}, $\mathcal{R}_{12}^{*R}$ and $\mathcal{R}_{12}^{*R}$.

– When $z_L > 1$ the 1-wave is a shock. Then, generalized jump conditions are used to compute S_L, v_{*L}, $\mathcal{R}_{12}^{*L}$ and $\mathcal{R}_{22}^{*L}$. Similarly, when $z_R > 1$, the generalized jump conditions are used to compute S_R, v_{*R}, $\mathcal{R}_{12}^{*R}$ and $\mathcal{R}_{22}^{*R}$.

– At this step, U_{*L} and U_{*R} are defined. Using the appropriate Riemann invariants of the 2-wave, we get v_{**}, $\mathcal{R}_{12}^{**}$ and $\mathcal{R}_{22}^{*L}$. The invariants for the 5-wave give $\mathcal{R}_{22}^{*R}$.

The computation of intermediate states is then completed.

5.3. Single shock solution

Given the left state $(h_L, u_L, v_L, \mathcal{P}_{11}^L, \mathcal{P}_{12}^L, \mathcal{P}_{22}^L)$, let us find a right state that is connected by a 1-shock. We will take a value of $z = h_R/h_L \in (1, 2)$. Then $h_R = zh_L$ and from the Hugoniot curve, we obtain

$$\mathcal{R}_{11}^R = (2h_R - h_L)\mathcal{R}_{11}^L/(2h_L - h_R) - \frac{1}{2}g(h_L - h_R)^3/(2h_L - h_R).$$

Then the velocity and shock speed are given by (5.8), (5.12)

$$u_{\mathrm{R}} = u_{\mathrm{L}} - \sqrt{\frac{(h_{\mathrm{R}} - h_{\mathrm{L}})(\mathrm{P}_{\mathrm{R}} - \mathrm{P}_{\mathrm{L}})}{h_{\mathrm{L}} h_{\mathrm{R}}}}, \quad S = u_{\mathrm{L}} - \sqrt{\frac{z}{2 - z}\left(3\mathcal{P}_{11}^{\mathrm{L}} + \frac{1}{2}gh_{\mathrm{L}}(3 - z)\right)}$$

where $\mathrm{P}_{\mathrm{L}}, \mathrm{P}_{\mathrm{R}}$ are the total pressures. The remaining quantities can be computed using the procedure in Section 5.1.

5.4. Vacuum states

A vacuum state refers to a zero value of water depth h and is also called a dry state. For classical shallow water model, Riemann problems with vacuum states can be solved with rarefaction waves [24, 27]. The velocity in the vacuum state is allowed to be non-zero which is not physically meaningful since there is no fluid in this state, but we seek a mathematically correct solution. For the SSW model, let us consider a left non-vacuum state $(h_{\mathrm{L}} > 0, \mathcal{R}^{\mathrm{L}} > 0)$ and a right vacuum state. In the vacuum state we also assume that the Reynolds tensor $\mathcal{P}^{\mathrm{R}} = 0$ and hence also $\mathcal{R}^{\mathrm{R}} = 0$. Let us first try to connect the states by a simple jump discontinuity moving at speed S. The jump condition of the h equation yields $0 - h_{\mathrm{L}} u_{\mathrm{L}} = S(0 - h_{\mathrm{L}})$ so that the discontinuity speed is $S = u_{\mathrm{L}}$. From the jump condition of the x momentum equation we get $0 - \left(\mathcal{R}_{11}^{\mathrm{L}} + h_{\mathrm{L}} u_{\mathrm{L}}^2 + \frac{1}{2}gh_{\mathrm{L}}^2\right) = S(0 - h_{\mathrm{L}} u_{\mathrm{L}}) = -h_{\mathrm{L}} u_{\mathrm{L}}^2$ so that $\mathcal{R}_{11}^{\mathrm{L}} + \frac{1}{2}gh_{\mathrm{L}}^2 = 0$, which implies that there is no solution.

We now try to connect the two states by a 1-rarefaction wave and make use of the invariants shown in equation (4.1). The second invariant yields $u_{\mathrm{R}} = u_{\mathrm{L}} + \mathfrak{a}(h_{\mathrm{L}}, c_{\mathrm{L}})$ and the sixth invariant yields $v_{\mathrm{R}} = v_{\mathrm{L}} + \frac{2\mathcal{P}_{12}^{\mathrm{L}}}{gh_{\mathrm{L}} + 2\mathcal{P}_{11}^{\mathrm{L}}}\mathfrak{a}(h_{\mathrm{L}}, c_{\mathrm{L}})$. Similarly, if the left state is a vacuum state and the right state is a non-vacuum state, they can be connected by a 6-rarefaction wave.

If an intermediate state is a vacuum state, say $h_{*\mathrm{L}} = 0$ then necessarily all the intermediate states in Figure 2 must be vacuum states, *i.e.*, $h_{*\mathrm{R}} = 0$, since shear/contact waves cannot connect a vacuum state to a non-vacuum state. The constancy of u in the intermediate states means that

$$u_{*\mathrm{L}} = u_{\mathrm{L}} + \mathfrak{a}(h_{\mathrm{L}}, c_{\mathrm{L}}) = u_{\mathrm{R}} - \mathfrak{a}(h_{\mathrm{R}}, c_{\mathrm{R}}) = u_{*\mathrm{R}}$$

i.e., we have equality in 5.5. The functions $g_{\pm}$ in this case are shown in Figure 5a which shows that the solution of $G(z_{\mathrm{L}}, z_{\mathrm{R}}) = 0$ is $z_{\mathrm{L}} = z_{\mathrm{R}} = 0$. On the other hand if $u_{\mathrm{R}} - u_{\mathrm{L}} > \mathfrak{a}(h_{\mathrm{L}}, c_{\mathrm{L}}) + \mathfrak{a}(h_{\mathrm{R}}, c_{\mathrm{R}})$ the functions $g_{\pm}$ are shown in Figure 5b and there is no solution to $G(z_{\mathrm{L}}, z_{\mathrm{R}}) = 0$. But we can still construct a solution with a 1-rarefaction and 6-rarefaction with an intermediate vacuum state, but it will not be possible to find a proper solution that satisfies all the structure of the intermediate states as shown in Figure 2, since $u_{*\mathrm{L}} \neq u_{*\mathrm{R}}$, see Figure 6. However the momentum is constant and zero in the intermediate state which may be considered as a solution that satisfies all the jump conditions, but the velocity in the intermediate states is not well defined. In this sense, the solution of the Riemann problem can be extended to include vacuum states. We note that the solutions described in the next Theorem are admissible weak solutions, since they are continuous in h, hv, E_{ij}, variables and they reduce to smooth solutions in the intermediate regions (the 2 rarefaction waves and the vacuum states). We summarise the solution with vacuum states in the following theorem.

Theorem 5.4. (1) *If the left state is non-vacuum state and the right state is a vacuum state such that* $u_{\mathrm{L}} + \mathfrak{a}(h_{\mathrm{L}}, c_{\mathrm{L}}) = u_{\mathrm{R}}$ *and* $v_{\mathrm{R}} = v_{\mathrm{L}} + \frac{2\mathcal{P}_{12}^{\mathrm{L}}}{gh_{\mathrm{L}} + 2\mathcal{P}_{11}^{\mathrm{L}}}\mathfrak{a}(h_{\mathrm{L}}, c_{\mathrm{L}})$, *then they can be connected by a 1-rarefaction wave.*
(2) *If the left state is a vacuum state and the right state is a non-vacuum state such that* $u_{\mathrm{L}} = u_{\mathrm{R}} - \mathfrak{a}(h_{\mathrm{R}}, c_{\mathrm{R}})$ *and* $v_{\mathrm{L}} = v_{\mathrm{R}} - \frac{2\mathcal{P}_{12}^{\mathrm{R}}}{gh_{\mathrm{R}} + 2\mathcal{P}_{11}^{\mathrm{R}}}\mathfrak{a}(h_{\mathrm{R}}, c_{\mathrm{R}})$, *then they can be connected by a 6-rarefaction wave.*
(3) *If* $u_{\mathrm{R}} - u_{\mathrm{L}} = \mathfrak{a}(h_{\mathrm{L}}, c_{\mathrm{L}}) + \mathfrak{a}(h_{\mathrm{R}}, c_{\mathrm{R}})$, *then they can be connected with a 1-rarefaction and 6-rarefaction wave with an intermediate vacuum state and velocity* $u_{*} = u_{\mathrm{L}} + \mathfrak{a}(h_{\mathrm{L}}, c_{\mathrm{L}}) = u_{\mathrm{R}} - \mathfrak{a}(h_{\mathrm{R}}, c_{\mathrm{R}})$. *(4) If* $u_{\mathrm{R}} - u_{\mathrm{L}} > \mathfrak{a}(h_{\mathrm{L}}, c_{\mathrm{L}}) + \mathfrak{a}(h_{\mathrm{R}}, c_{\mathrm{R}})$, *then they can be connected with a 1-rarefaction and 6-rarefaction wave with an intermediate vacuum state, see Figure 6.*
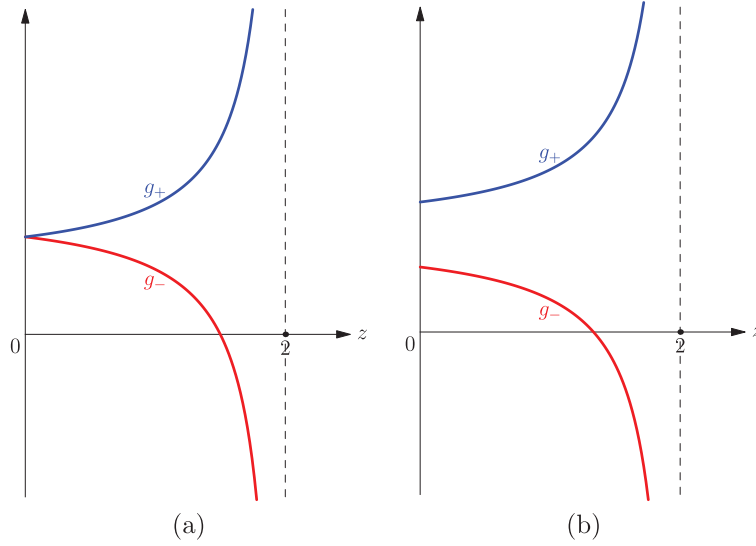
FIGURE 5. Illustration of the functions $g_\pm$ leading to intermediate vacuum state in the Riemann problem. (a) $u_R - u_L = \mathfrak{a}(h_L, c_L) + \mathfrak{a}(h_R, c_R)$, (b) $u_R - u_L > \mathfrak{a}(h_L, c_L) + \mathfrak{a}(h_R, c_R)$.
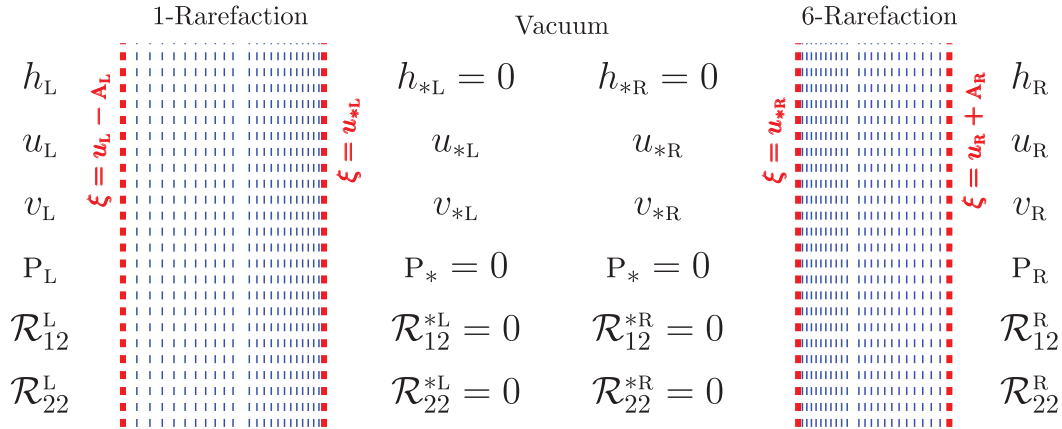

FIGURE 6. Shear Shallow Water (SSW) model: Wave structure of the 1-D Riemann problem in presence of vacuum, when $u_R - u_L \geq \mathfrak{a}(h_L, c_L) + \mathfrak{a}(h_R, c_R)$. Formally, without giving it a physical meaning because the depth and momentum are zero, we can define the velocities of intermediate states as : $u_{*L} = u_L + \mathfrak{a}(h_L, c_L)$, $v_{*L} = v_L + \frac{2\mathcal{P}_{12}^L}{gh_L + 2\mathcal{P}_{11}^L}\mathfrak{a}(h_L, c_L)$, $u_{*R} = u_R - \mathfrak{a}(h_R, c_R)$ and $v_{*R} = v_R - \frac{2\mathcal{P}_{12}^R}{gh_R + 2\mathcal{P}_{11}^R}\mathfrak{a}(h_R, c_R)$.

6. BRIEF DESCRIPTION OF PATH CONSERVATIVE SCHEMES

We refer the reader to Parés [23] for a good general introduction to the concept of path conservative numerical schemes for non-conservative systems, and to Chandrashekar *et al.* [9] for a discussion specific to the present model. The Riemann problem is the building block of a finite volume method and this approach can be used for non-conservative systems also [18,23]. The main idea is to split the *fluctuation* into two parts corresponding

to left moving and right moving waves arising in the Riemann solution, where the fluctuation is defined as

$$\boldsymbol{D}(\boldsymbol{U}_{\mathrm{L}}, \boldsymbol{U}_{\mathrm{R}}) = \int_0^1 \boldsymbol{A}(\Psi(\xi; \boldsymbol{U}_{\mathrm{L}}, \boldsymbol{U}_{\mathrm{R}})) \frac{\mathrm{d}\Psi}{\mathrm{d}\xi}(\xi; \boldsymbol{U}_{\mathrm{L}}, \boldsymbol{U}_{\mathrm{R}}) \mathrm{d}\xi = \boldsymbol{D}^-(\boldsymbol{U}_{\mathrm{L}}, \boldsymbol{U}_{\mathrm{R}}) + \boldsymbol{D}^+(\boldsymbol{U}_{\mathrm{L}}, \boldsymbol{U}_{\mathrm{R}}).$$

The splitting of the fluctuation can be performed using a Roe-type Riemann solver or HLL-type Riemann solver, the latter being the approach taken in the present work and following Chandrashekar $et\ al.$ [9]. HLL-type methods model the Riemann solution by simple waves and require estimation of the smallest and largest wave speed arising in the Riemann problem. Assume that there are m simple waves in the approximate Riemann solution with $m-1$ intermediate states. Let us denote the wave speeds as S_j, $j = 1, \ldots, m$ and the intermediate states as $\boldsymbol{U}_j^*$, $j = 1, \ldots, m-1$ with $\boldsymbol{U}_0^* = \boldsymbol{U}_{\mathrm{L}}$ and $\boldsymbol{U}_m^* = \boldsymbol{U}_{\mathrm{R}}$. The fluctuation splitting is given by

$$\boldsymbol{D}^\pm(\boldsymbol{U}_{\mathrm{L}}, \boldsymbol{U}_{\mathrm{R}}) = \sum_{j=1}^m S_j^\pm \left(\boldsymbol{U}_{j+1}^* - \boldsymbol{U}_j^*\right)$$

where

$$S^- = \min(0, S), \quad S^+ = \max(0, S).$$

The intermediate states are obtained by satisfying the Rankine–Hugoniot conditions across all the waves. The approximate Riemann solvers of different complexity based on the number of waves including in the model can be derived. In Chandrashekar $et\ al.$ [9], two wave HLL solver, three wave HLLC3 solver and five wave HLLC5 approximate Riemann solvers have been constructed by using the generalized jump conditions. The HLL solver contains only the slowest and fastest waves in its model; the HLLC3 solver also includes the contact wave while the HLLC5 solver includes all five waves.

Let us consider a partition of the domain into disjoint cells of size Δx. Let $\boldsymbol{U}_j^n$ denote the approximation of the cell average value in the jth cell at time $t = t_n$. The first order scheme is given by

$$\boldsymbol{U}_j^{n+1} = \boldsymbol{U}_j^n - \frac{\Delta t}{\Delta x}\left(\boldsymbol{D}_{j-\frac{1}{2}}^{+,n} + \boldsymbol{D}_{j+\frac{1}{2}}^{-,n}\right) + \Delta t \boldsymbol{S}(\boldsymbol{U}_j^{n+\theta}), \quad \boldsymbol{D}_{j+\frac{1}{2}}^{\pm,n} = \boldsymbol{D}^\pm\left(\boldsymbol{U}_j^n, \boldsymbol{U}_{j+1}^n\right).$$

For $\theta = 0$ we obtain an explicit scheme and for $\theta = 1$ we obtain a semi-implicit scheme; however the coupling in the semi-implicit scheme is only local to the cell. An exact solution process for the semi-implicit scheme is explained in the Appendix of Chandrashekar $et\ al.$ [9]. If the system is conservative, $i.e.$, $\boldsymbol{A} = \boldsymbol{F}'(\boldsymbol{U})$ for some $\boldsymbol{F}$, then the above scheme can be written in conservation form with some numerical flux function [23]. Such a scheme can be made higher order accurate using a MUSCL-Hancock approach as in Chandrashekar $et\ al.$ [9] or using a method of lines approach combined with a high order Runge-Kutta scheme. The numerical computations used in this work are based on a MUSCL-Hancock approach as explained in Chandrashekar $et\ al.$ [9].

6.1. Estimation of wave speeds

The approximate Riemann solver requires an estimate of the slowest and fastest wave speeds which should enclose the exact wave speeds in order for the entropy condition to be satisfied. One commonly used method to estimate the wave speeds in the Riemann problem uses a combination of the left and right states and the Roe average state [14]; following this idea we can use the following speed estimates

$$S_{\mathrm{L}}^{\mathrm{HLL}} = \min\left\{\lambda_1(\boldsymbol{Q}_{\mathrm{L}}), \lambda_1(\bar{\boldsymbol{Q}})\right\}, \quad S_{\mathrm{R}}^{\mathrm{HLL}} = \max\left\{\lambda_6(\boldsymbol{Q}_{\mathrm{R}}), \lambda_6(\bar{\boldsymbol{Q}})\right\}, \quad \bar{\boldsymbol{Q}} = \frac{1}{2}(\boldsymbol{Q}_{\mathrm{L}} + \boldsymbol{Q}_{\mathrm{R}})$$

where $\boldsymbol{Q}$ represents the variables $(h, \boldsymbol{v}, \mathcal{R})$ and we use the arithmetic average instead of the Roe average. If S_{L}^{ex}, S_{R}^{ex} denote the exact wave speeds, then we require that $S_{\mathrm{L}}^{\mathrm{HLL}} \le S_{\mathrm{L}}^{ex}$ and $S_{\mathrm{R}}^{\mathrm{HLL}} \ge S_{\mathrm{R}}^{ex}$, but this is not guaranteed to hold with the above estimates. As an example, consider the dam break problem from Section 7.1 for which the slowest and fastest speeds are

$$S_{\mathrm{L}}^{ex} = -0.44328320518603004, \quad S_{\mathrm{R}}^{ex} = 0.43554139386439333$$

whereas the speed estimate obtained from the above formulae are

$$S_{\mathrm{L}}^{\mathrm{HLL}} = -0.44328320518603004, \quad S_{\mathrm{R}}^{\mathrm{HLL}} = 0.38399218742052554.$$

We see that fastest speed S_{R} is very much under estimated and this may cause numerical problems like loss of positivity and violation of entropy condition. How to obtain better estimates of the slowest and fastest speeds without using the exact Riemann solution is an open question. In the present work we use a simple way to over-estimate the speeds by using both the states to estimate the speeds as follows

$$S_{\mathrm{L}}^{\mathrm{HLL}^*} = \min\{\lambda_1(\boldsymbol{Q}_{\mathrm{L}}), \lambda_1(\boldsymbol{Q}_{\mathrm{R}}), \lambda_1(\bar{\boldsymbol{Q}})\}, \quad S_{\mathrm{R}}^{\mathrm{HLL}^*} = \max\{\lambda_6(\boldsymbol{Q}_{\mathrm{L}}), \lambda_6(\boldsymbol{Q}_{\mathrm{R}}), \lambda_6(\bar{\boldsymbol{Q}})\}. \tag{6.1}$$

For the dam break problem, this yields

$$S_{\mathrm{L}}^{\mathrm{HLL}^*} = -0.44328320518603004, \quad S_{\mathrm{R}}^{\mathrm{HLL}^*} = 0.44328320518603004.$$

Now the fastest speeds is also estimated in such a way that the numerical Riemann fan bounds the exact Riemann fan. We use the above estimate in all the approximate Riemann solvers used in this study.

7. Exact solutions compared with approximate Riemann solvers

In the next few sections, we compare the exact solutions with numerical solutions obtained with approximate Riemann solvers using a second order accurate MUSCL-Hancock scheme [9]. Unless stated otherwise, we use the speed estimates given by (6.1) in all the test cases. We show results obtained from second order numerical scheme in most of the test cases since we do not observe any qualitative difference between first and second order results, but in some test cases, where significant differences are found, we show first order results also. In all the tests, the bottom topography is constant and the source term $\boldsymbol{S}$ is absent, since we want to study the purely hyperbolic problem.

7.1. Dam break problem

We consider here the test case used in Bhole *et al.* [3], Gavrilyuk *et al.* [15] and Chandrashekar *et al.* [9]. It is a Riemann problem where, initially, the velocity is zero every where, the stress tensor is constant and only the initial depth has a jump,

$$h = \begin{cases} 0.02, \, x < 0.5 \\ 0.01, \, x > 0.5 \end{cases}, \quad u = 0, \quad v = 0, \quad \mathcal{P}_{11} = 10^{-4}, \quad \mathcal{P}_{12} = 0, \quad \mathcal{P}_{22} = 10^{-4}.$$

For this Riemann data, we can compute the associated analytical solution. Numerical approximations are performed with HLL and HLLC (3-waves and 5-waves) Riemann solvers (see [9] for details). Figure 7 shows that the exact and the approximate solutions are almost comparable, except for the shock front. The HLL and HLLC Riemann solvers are converging to the same limit. However, in accordance with Chandrashekar *et al.* [9], the numerical limit does not match with the exact solution as seen in Figure 8. This is probably related to the fact that $\mathcal{P}_{11}$ is too small; initially we have $\mathcal{P}_{11} = 10^{-4}$ and $\mathrm{c} = \sqrt{\mathcal{P}_{11}} = 10^{-2}$. Indeed, as c goes to zero, the shear and the contact waves approach one another and they coincide in the limit of $\mathcal{P}_{11} = 0$. The Riemann solvers used here are not designed to get the proper behaviour at this asymptotic case. The approximate Riemann solvers used here are not designed to strictly conserve the total energy (2.4). As shown in Theorem 3.1, the jump condition of total energy equation is automatically satisfied by the jump conditions of the SSW model. The approximate Riemann solver is based on satisfying these jump conditions and we can expect approximate conservation in the numerical scheme also. To examine the conservation of total energy in the domain, we plot it as a function of time in Figure 10, where the ratio of total energy at time t to that at initial time is shown. We see that it is not strictly conserved by the numerical scheme but there is a dissipation of this energy, with the error at the final time being about 0.15% on the coarse mesh. At the PDE level, the
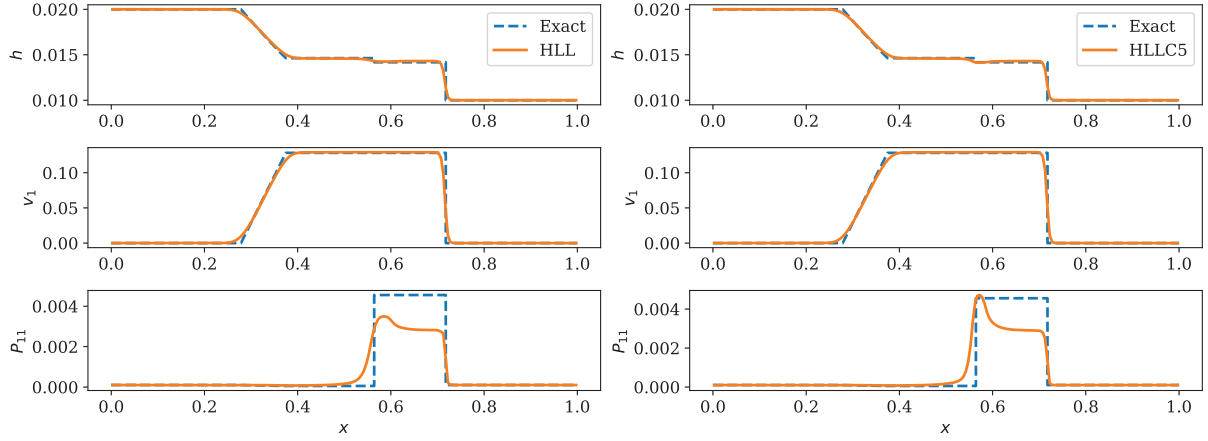
FIGURE 7. Dam break test case with 200 cells and second order approximations. Comparison between exact and numerical solutions obtained with HLL (*left*) and HLLC5 (*right*) schemes.
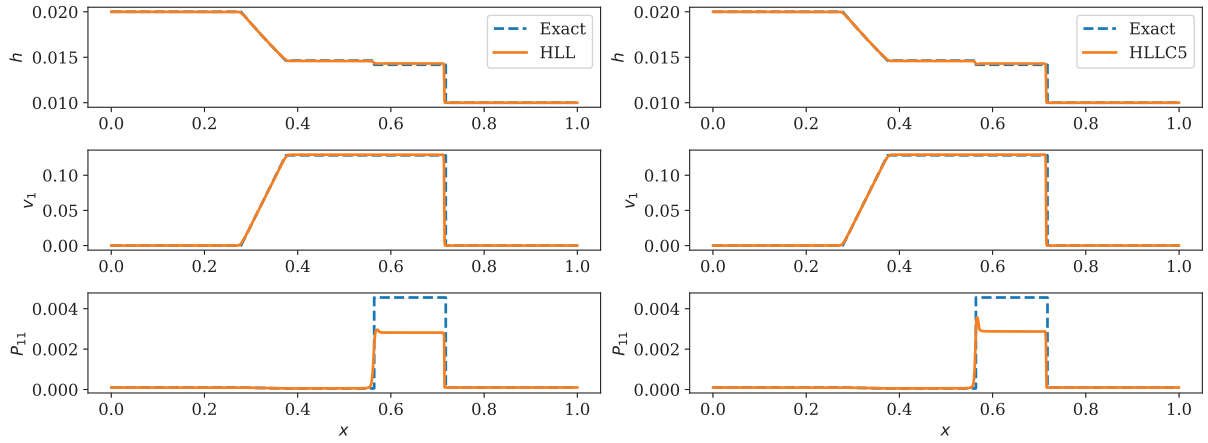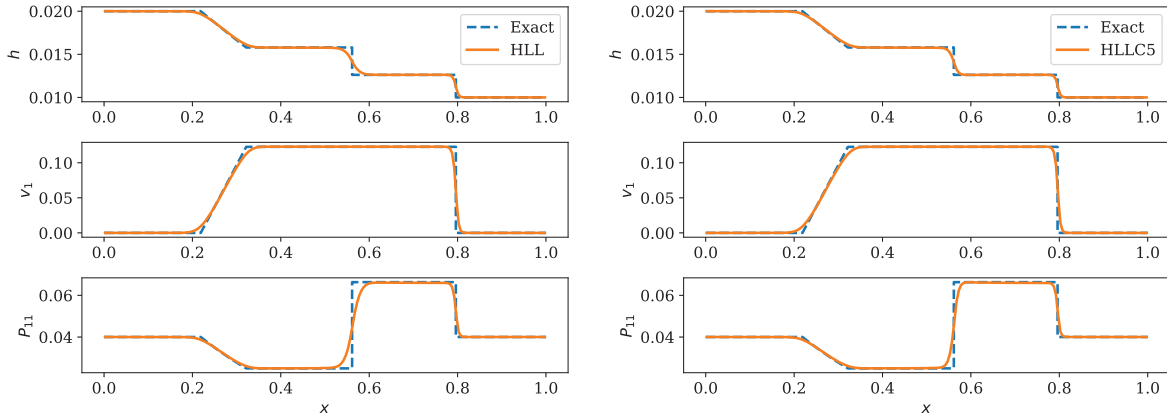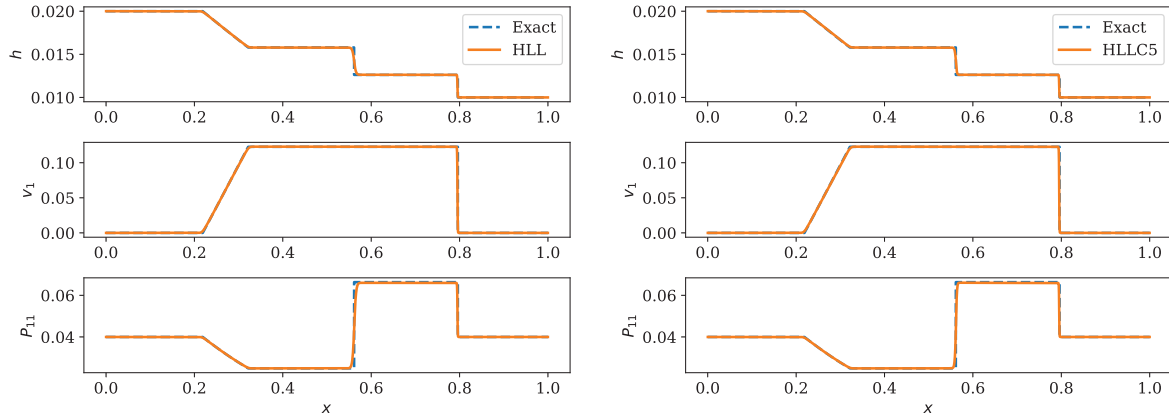

FIGURE 8. Dam break test case with 2000 cells and second order approximations. Comparison between exact and numerical solutions obtained with HLL (*left*) and HLLC5 (*right*) schemes.

total energy is conserved for inviscid problems ($\mathcal{D} = 0$). At the discrete level, this property is satisfied if we solve the conservative form of the total energy, which is not the case here. Nevertheless, it is possible to strengthen this conservation law, either by using an augmented system [15] or by redistributing the energy conservation defect on the pressure tensor as done in Busto *et al.* [4].

A modified test case has been designed in order to keep $\mathcal{P}_{11}$ away from zero. The Riemann data is given by

$$h = \begin{cases} 0.02, \ x < 0.5 \\ 0.01, \ x > 0.5 \end{cases}, \quad u = 0, \quad v = 0, \quad \mathcal{P}_{11} = 4 \times 10^{-2}, \quad \mathcal{P}_{12} = 0, \quad \mathcal{P}_{22} = 4 \times 10^{-2}.$$

In this modified context the numerical solution does not contain any more defect in the shock front propagation with respect to the exact solution, even at low numerical resolution as shown in Figure 9. The convergence to the analytical solution is also observed in Figures 11 and 9. Thus it seems that we are facing here a lack of asymptotic preserving property of the numerical schemes when $\mathcal{P}_{11}$ goes to zero. At this asymptotic, the shock

FIGURE 9. Modified dam break test case with 200 cells and second order approximations. Comparison between exact and numerical solutions obtained with HLL (*left*) and HLLC5 (*right*) schemes.
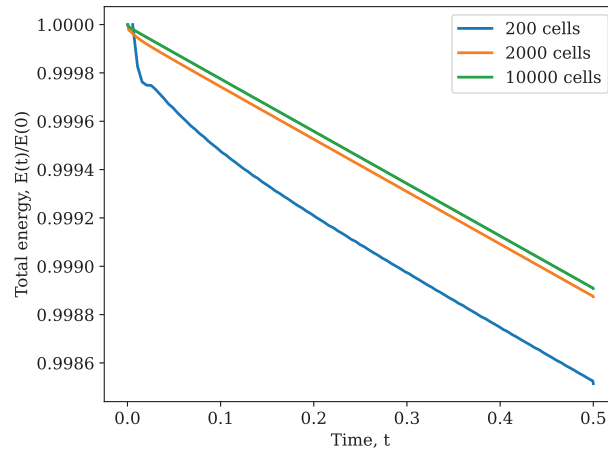
FIGURE 10. Total energy in the domain as a function of time for dam break problem using HLLC5 scheme.

front seems to be not accurately resolved with the current schemes, when compared with the designed exact solution. Note that disagreement only occurs at the shock front and elsewhere the numerical approximations converge to the analytical solution. The convergence is observed even at the shock front when the value of $\mathcal{P}_{11}$ is not too small. Similar convergence is also observed if we use $\mathcal{P}_{11} = 4 \times 10^{-2}$, $\mathcal{P}_{12} = 0$ and $\mathcal{P}_{22} = 10^{-8}$.

We also test another variant of the modified dam break problem, where $\mathcal{P}_{12}$ is set to a small non zero value,

$$h = \begin{cases} 0.02, \, x < 0.5 \\ 0.01, \, x > 0.5 \end{cases}, \quad u = 0, \quad v = 0, \quad \mathcal{P}_{11} = 4 \times 10^{-2}, \quad \mathcal{P}_{12} = 10^{-8}, \quad \mathcal{P}_{22} = 4 \times 10^{-2}.$$

The numerical approximation, even on a coarse mesh as shown in Figure 14, fit very well with the designed exact solution. With this modification, the profile of $\mathcal{P}_{12}$ shows all the five waves of the SSW system. As expected, the intermediate waves are better resolved by the HLLC schemes.
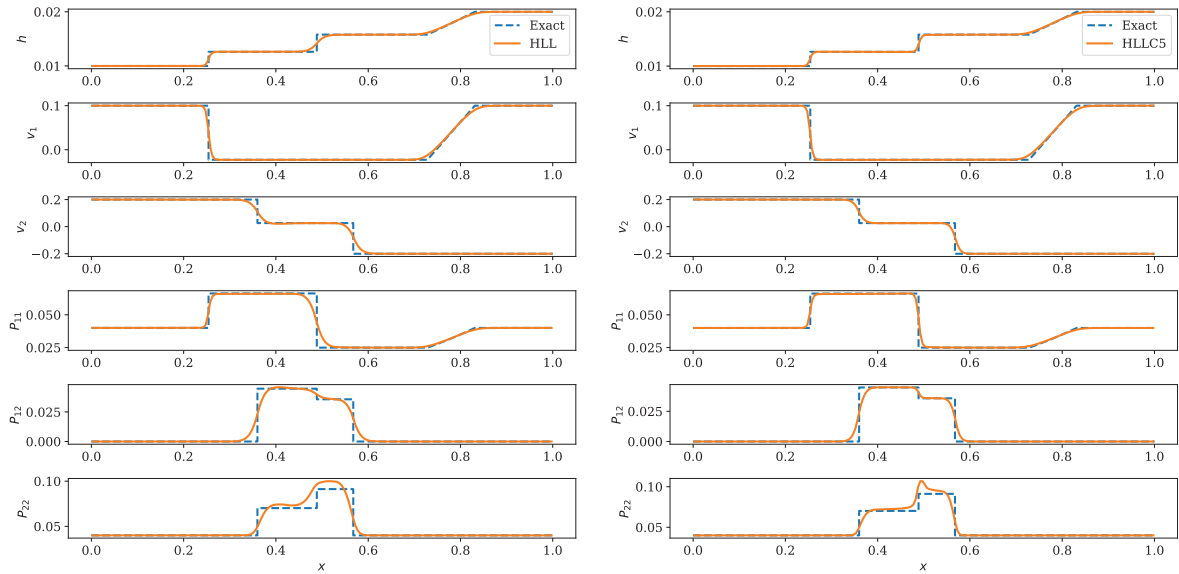
FIGURE 11. Modified dam break test case with 2000 cells and second order approximations. Comparison between exact and numerical solutions obtained with HLL (*left*) and HLLC5 (*right*) schemes.
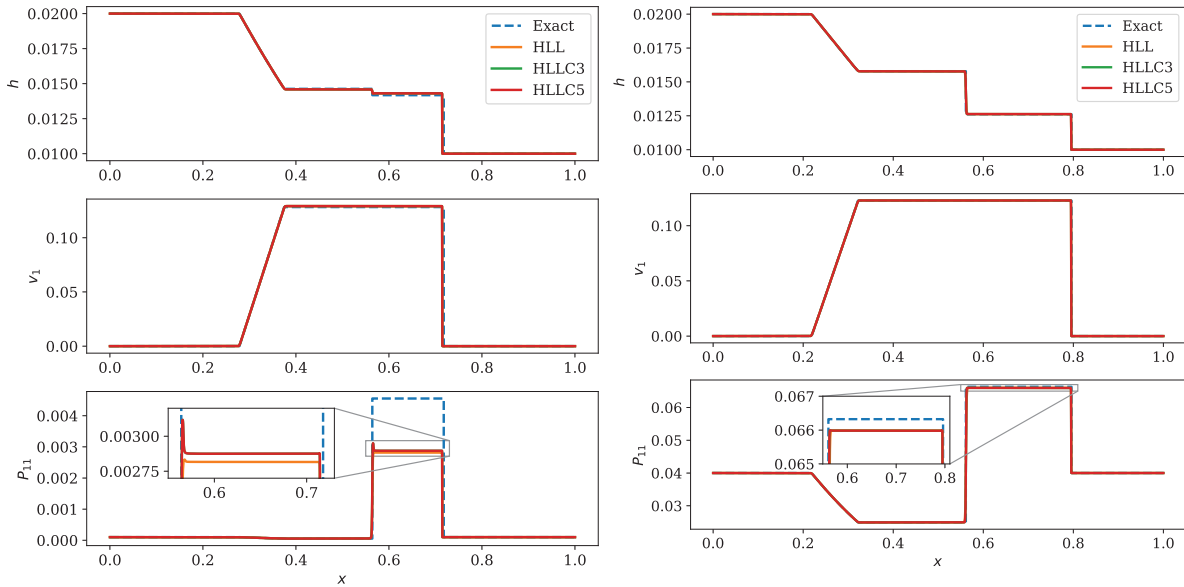

FIGURE 12. Converged solutions for dam break (*left*) and modified dam break (*right*) problems. Numerical solutions are shown with 10 000 cells.

As shown in Figure 12, the mesh convergence is observed for the three Riemann solvers used, both for the dam break and for the modified dam break problems. Indeed, the different numerical approaches converge asymptotically to the same numerical solution, as the mesh becomes more and more refined. Nevertheless, for the initial dam break problem, the numerical solutions converge to a different solution than the one obtained analytically as seen in the left figure; with the HLL solution being slightly different from the HLLC solvers. On the other hand, for the modified dam break problem shown on the right, where the determinant of $\mathcal{P}$ is not as close to zero, the numerical solutions overlap closely with the analytical solution. However, there is still a small difference in the $\mathcal{P}_{11}$ values around the shock as shown in the inset figure. The convergence of the L^1 errors with
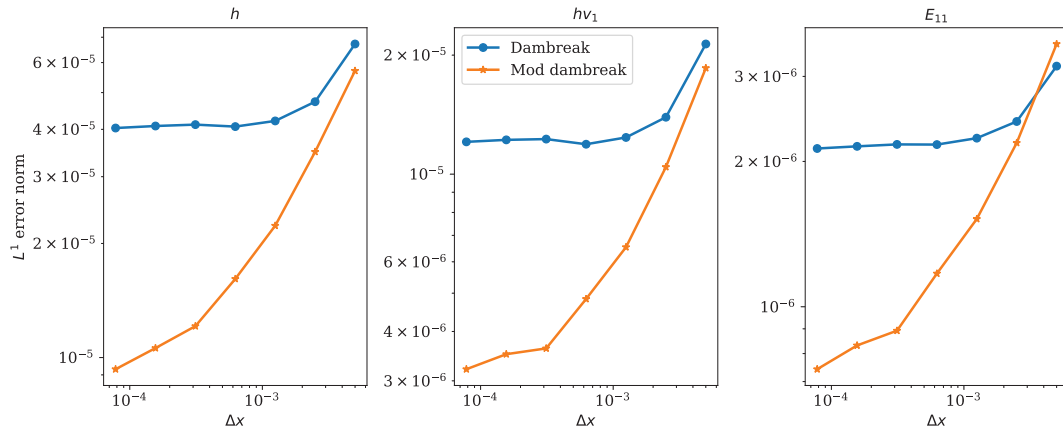
FIGURE 13. Convergence of L^1 error norm for dambreak problems using HLLC5 scheme
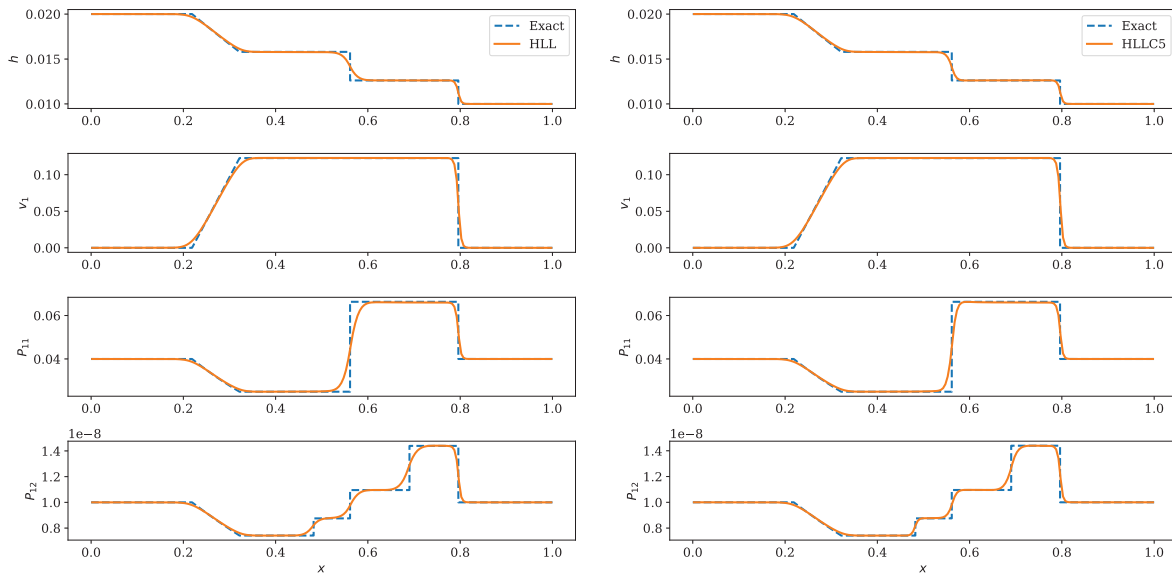
FIGURE 14. Modified dam break with initially $\mathcal{P}_{12} = 10^{-8}$ in the entire domain. Mesh of 200 cells and second order approximations. Comparison between exact and numerical solutions obtained with HLL (*left*) and HLLC5 (*right*) schemes.

respect to the exact solution are shown in Figure 13 where we see that both test cases converge to a solution different from the exact solution. The modified dam break case converges to smaller errors but eventually the convergence stalls, which is expected since we have already observed this in Figure 12.

7.2. Five waves dam break problem

The initial condition for the Riemann problem is given in the following table.

	h	v_1	v_2	$\mathcal{P}_{11}$	$\mathcal{P}_{12}$	$\mathcal{P}_{22}$
$x < 0.5$	0.01	0.1	0.2	4×10^{-2}	10^{-8}	4×10^{-2}
$x > 0.5$	0.02	0.1	-0.2	4×10^{-2}	10^{-8}	4×10^{-2}

FIGURE 15. Five waves dam break test case with 200 cells and second order approximations. Comparison between exact and numerical solutions obtained with HLL (*left*) and HLLC (*right*) schemes.
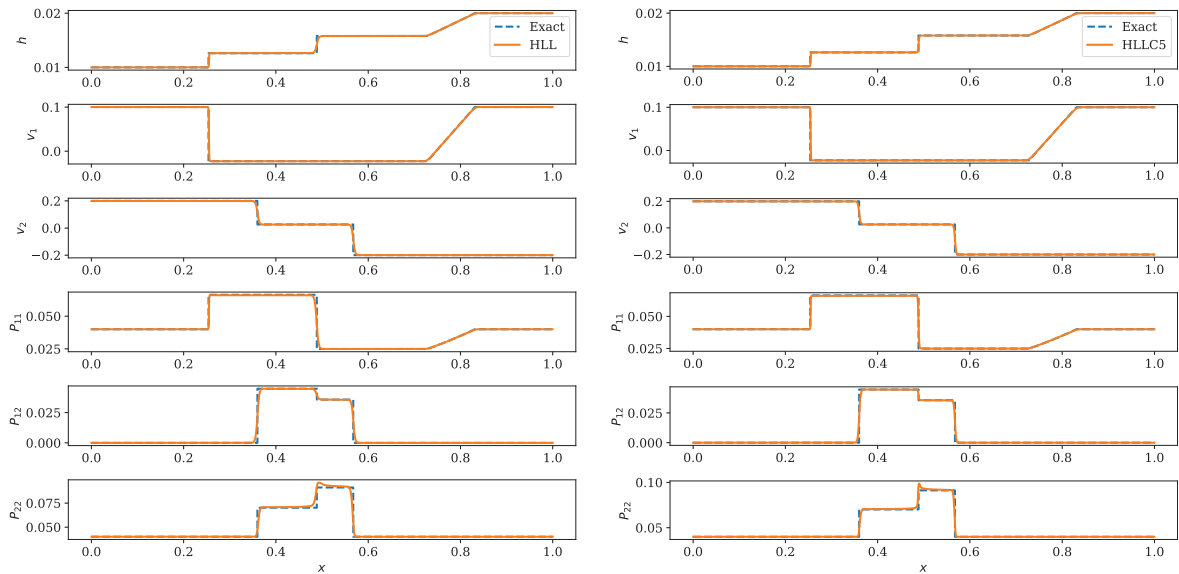
FIGURE 16. Five waves dam break test case with 2000 cells and second order approximations. Comparison between exact and numerical solutions obtained with HLL (*left*) and HLLC (*right*) schemes.

The initial data is like a dam break problem but with some initial shear v and a non-zero normal velocity u. The results are shown in Figures 15 and 16 at time $t = 0.5$ units. The solution shows five waves including 1-shock and 6-rarefaction wave. All the waves are captured by both Riemann solvers even on the coarse mesh
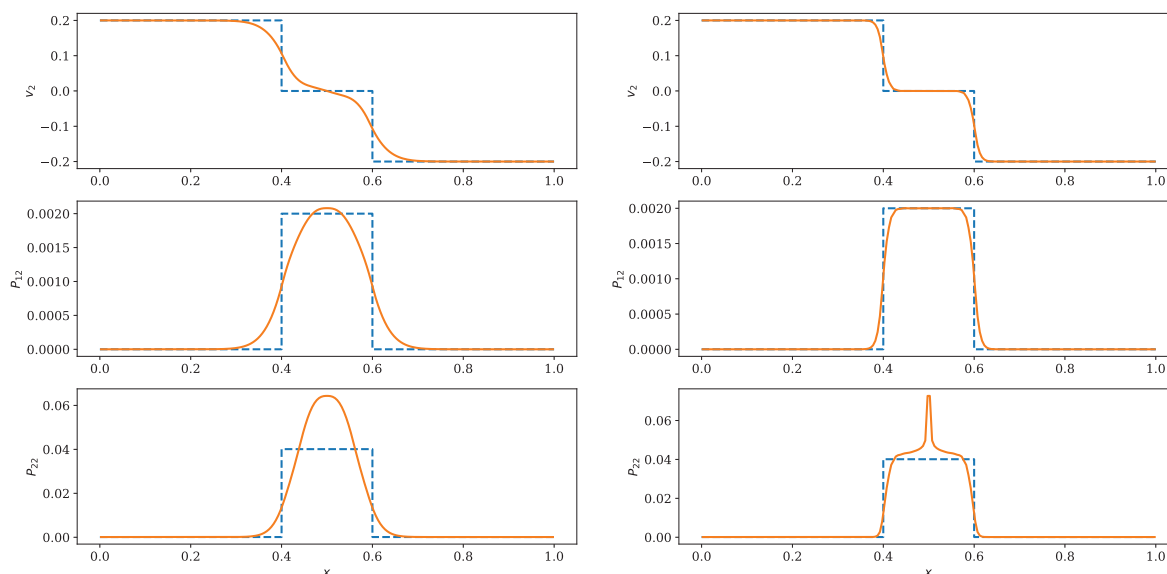
FIGURE 17. Shear test case with 200 cells and second order approximations. Comparison between exact and numerical solutions obtained with HLL (*left*) and HLLC5 (*right*) schemes.
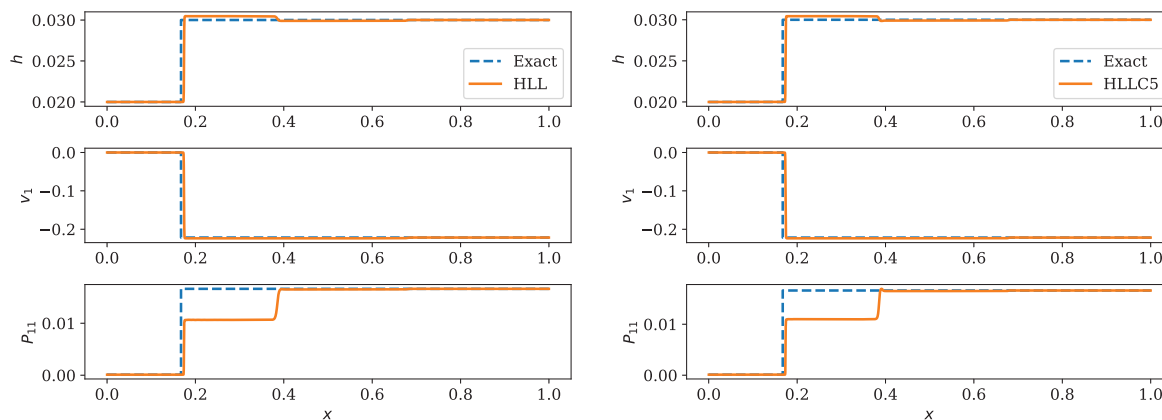
FIGURE 18. Single moving shock test case on 2000 cells.

of 200 cells. The numerical solution and the location of the waves agrees well with the exact solution, and the numerical results approach the exact solution on the finer mesh as seen in Figure 16. The values of $\mathcal{P}$ used are larger as in the case of the modified dam break problem and this leads to good agreement between the numerical and exact solutions, which was observed in the previous dam break problem.

7.3. Shear waves problem

The initial condition for the Riemann problem is given in the following table.

	h	v_1	v_2	$\mathcal{P}_{11}$	$\mathcal{P}_{12}$	$\mathcal{P}_{22}$
$x < 0.5$	0.01	0.0	0.2	10^{-4}	0.0	10^{-4}
$x > 0.5$	0.01	0.0	-0.2	10^{-4}	0.0	10^{-4}
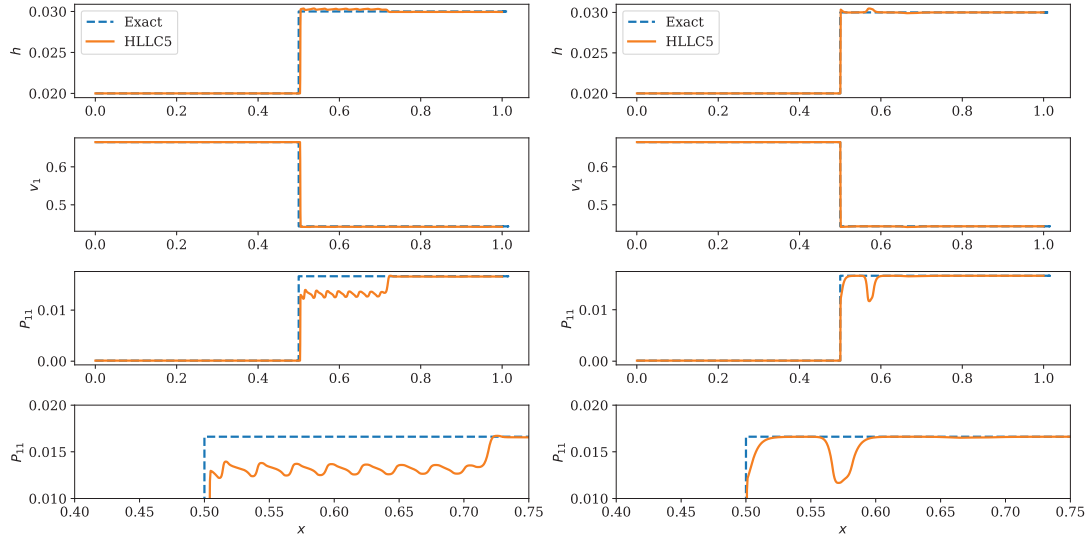
FIGURE 19. Single stationary shock test case on 2000 cells using approximate speed (*left*) and exact speeds (*right*).

The result is shown in Figure 17 at time $t = 10$ on a mesh of 200 cells, where we see two shear waves in the solution. The numerical solution including the location of the waves agrees well with the exact solution. The HLLC5 solver gives a better resolution of the shear waves since they are included in the approximate wave model. However, there are spurious spikes found at the center in $\mathcal{P}_{22}$ where there is a stationary contact discontinuity. This behavior is similar to what is usually observed with numerical solution of some Riemann problems for the compressible Euler flows.

7.4. Single shock wave problem

In this test case, we use a Riemann data for which the exact solution consists of a single shock wave, as described in Section 5.3. The initial condition is given by

	h	v_1	v_2	$\mathcal{P}_{11}$	$\mathcal{P}_{12}$	$\mathcal{P}_{22}$
$x < 0.5$	0.02	0	0	10^{-4}	0	10^{-4}
$x > 0.5$	0.03	-0.22169799277395363	0	0.016616666666666658	0	10^{-4}

Figure 18 shows the numerical solution obtained with the HLLC5 solver on a mesh of 2000 cells. While the shock location matches closely, we see that the numerical solutions exhibit an extra contact wave which is not present in the exact solution. All solvers exhibit this behavior and this is seen even under grid refinement. This situation is similar to the dambreak problem where the solution of $\mathcal{P}_{11}$ does not agree with the exact solution.

We next consider the same problem but solve it in a frame where the exact shock is stationary. The corresponding Riemann data is given by

	h	v_1	v_2	$\mathcal{P}_{11}$	$\mathcal{P}_{12}$	$\mathcal{P}_{22}$
$x < 0.5$	0.02	0.6650939783218609	0	10^{-4}	0	10^{-4}
$x > 0.5$	0.03	0.44339598554790727	0	0.016616666666666658	0	10^{-4}

We solve this problem using the speed estimates given in (6.1) and also using the exact speeds obtained from the exact Riemann solver. Figure 19 shows the two sets of results on a mesh of 2000 cells; with the approximate speeds, we see a similar wave pattern as in the moving shock case, but there are many dispersive waves seen between the shock and the contact, as seen in the bottom figure which shows a zoomed view of $\mathcal{P}_{11}$. When the
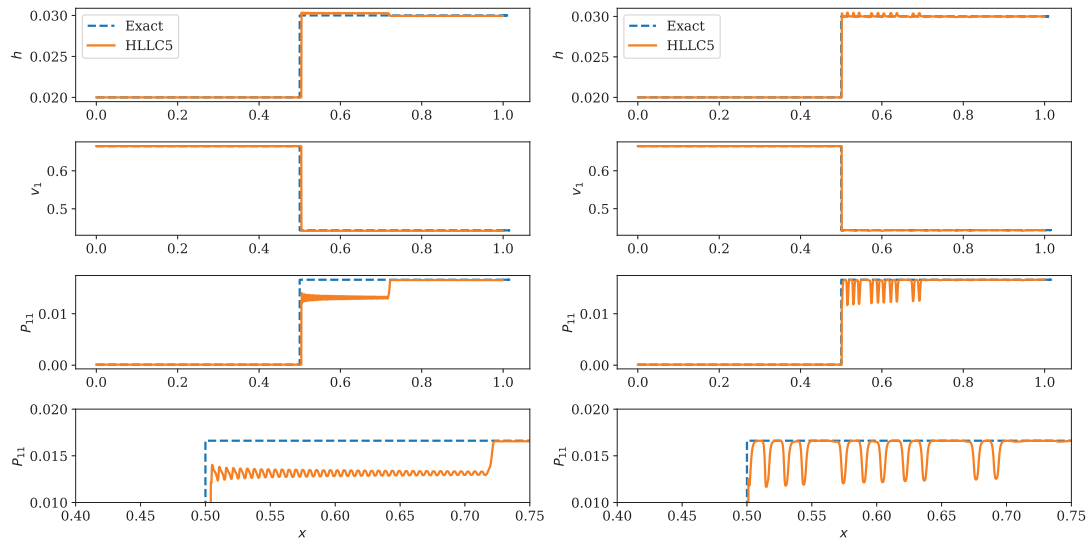
FIGURE 20. Single stationary shock test case on 10 000 cells using approximate speed (*left*) and exact speeds (*right*).

exact speeds are used, as shown in the right of Figure 19, we see a better agreement with the exact solution but there are still some extra waves present in the numerical solution. Figure 20 shows the results obtained with a refined mesh of 10 000 cells. The numerical solver based on approximated wave speeds behaves almost as a dispersive shock that is usually associated to modulated wave-train. It seems that, as soon as the shock cannot be numerically resolved without any dissipation, the numerical solution can be different from the analytical one. In other words, the shocks obtained with dissipative numerical schemes and those obtained analytically with the same generalized jump conditions, do not perfectly coincide. This problem of convergence failure has been analyzed in Castro *et al.* [5] using the modified equation. It was shown that this non-intuitive behavior is due to numerical viscosity and/or numerical dispersion. Therefore, as far as the numerical scheme involves some dissipation, they will converge to a solution that depend, not only on the chosen path family, but also and especially on the specific form of its dissipation terms, whereas the analytical solution will be determined only by the choice of the path family. This discrepancy between the numerical and analytical solutions is one of the peculiarities of non-conservative systems. The results we obtain here, plotted for example on Figures 12, 19–21, support the overall trend described in Castro *et al.* [5]. The two first order results obtained with approximate and exact wave speeds almost coincide in Figure 21 and we cannot visually distinguish them. However, contrary to the first order accurate scheme in Figure 21, when the second order method is used in Figures 19–21, we can observe on the variable $\mathcal{P}_{11}$ a wave train, going to the right, generated at the location of the stationary shock. The structure of this wave train is different depending on whether the wave velocities used in the Riemann solver are exact or approximate. This suggests that, in this context, the numerical diffusion becomes residual and we probably observe here a behavior specific to numerical schemes whose modified equations are dominated by dispersion [16]. This trend will be analyzed and quantified in future work.

7.5. Single contact wave problem

The Riemann data for this problem is given by

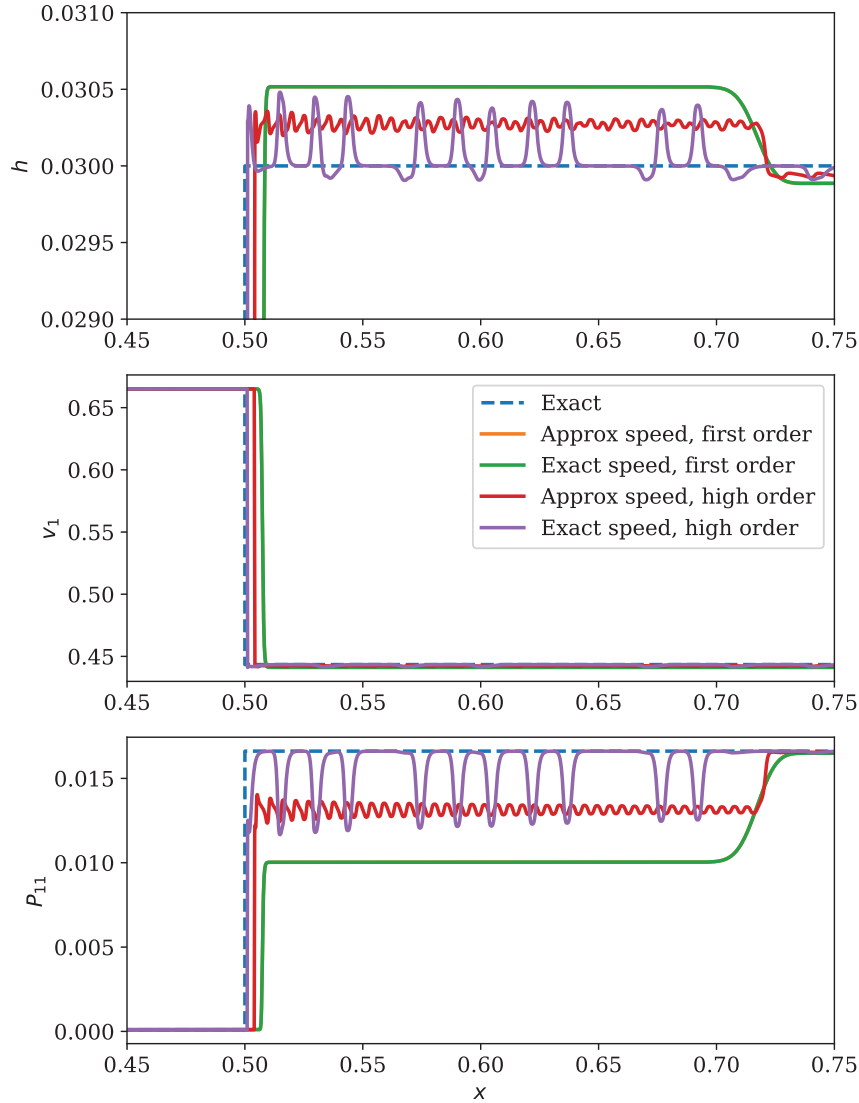|	h	v_1	v_2	$\mathcal{P}_{11}$	$\mathcal{P}_{12}$	$\mathcal{P}_{22}$
$x < 0.5$	0.02	0.1	0	10^{-4}	0	10^{-4}
$x > 0.5$	0.01	0.1	0	0.014735	0	2×10^{-4}

FIGURE 21. Single stationary shock test case using 10 000 cells; first and second order schemes using approximate and exact speeds.

which gives rise to a single contact wave in the exact solution. Since the water depth h has a jump, the non-conservative terms are non-zero in this case. Figure 22 shows the solution at time $t = 2.5$ obtained using the three approximate Riemann solvers on a mesh of 2000 cells. The solution and the location of the contact wave is captured well by all the numerical schemes. The HLL solver introduces more numerical dissipation since it does not explicitly model the contact wave, while both HLLC3 and HLLC5 solvers include this wave in their model and give very similar results. Contrary to the simple shock case, the numerical and analytical contact discontinuity coincide perfectly, despite the numerical approximation of the path (several points in the numerical discontinuity). Indeed, the contact discontinuity is a linearly degenerate wave and its associated states are defined by the Riemann invariants that we have obtained explicitly and independently of the path.
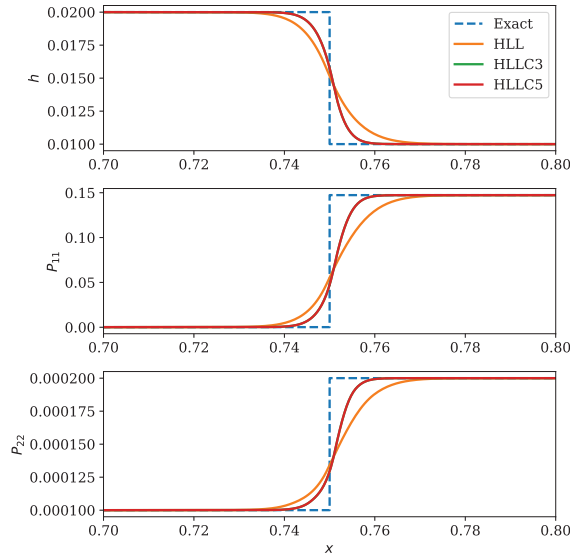
FIGURE 22. Single contact test case on 2000 cells. Comparison of three different Riemann solvers with the exact solution.

8. SUMMARY AND CONCLUSIONS

We have derived the exact solution of the Riemann problem for the non-conservative model of shear shallow water flows. The PDE is written in an almost conservative form that is very close to the 10-moment model for gas dynamics and admits a convex entropy function. The notion of solution is based on path conservative approach for which a path has to be assumed. In the numerical approaches, a linear path in the space of conserved variables is usually assumed and we derive the exact solution for this linear path. Several test cases are given and the numerical results are compared with the exact solution. In some problems as in dam break case, we see that the numerical solution of $\mathcal{P}$ does not agree with the exact solution, though wave locations are predicted correctly. When the stress levels $\mathcal{P}$ are not too small, the agreement is much better as seen in the modified dam break problem. In the case of single shock problem, the numerical solutions produce an extra contact wave; the solutions depend sensitively on the choice of the speed estimates used in the HLL solvers. When the exact speeds are used for the stationary shock problem, there is better agreement but we observe several other waves which may indicate that the numerical strategies in this context are, locally around the shocks, dominated by dispersion rather than dissipation.

We must also remember that the exact solution depends on the choice of the path and even when the path is fixed, the numerical shocks my be different to the exact one. Nevertheless, apart from the shocks profile for which significant differences are observed, for all other waves (contact discontinuity, shear waves and rarefaction waves) the numerical solution converges well to the exact solution. The difficulties observed for the shock waves raise the problem of the stability of the shocks in the framework of non-conservative hyperbolic equations, for a given path (approximated Rankine Hugoniot conditions). To give a solid explanation, it will probably be necessary to carry out a thorough study of the stability of *non-conservative shocks*, which is beyond the scope of this paper.

APPENDIX A. NUMERICAL SOLUTION OF ROOT FINDING PROBLEM

The solution of (5.3) is obtained numerically by applying a Newton method. The algorithm for the Newton method is as follows. Define $z = (z_L, z_R)$ and $H(z) = [F(z), G(z)]^\top$. Set the tolerance $\epsilon = 10^{-6}$. We start at the point $z = (1, 1)$.

(1) If $|F(z)| < \epsilon$ and $|G(z)| < \epsilon$, then stop.
(2) Solve $H'(z)\Delta z = -H(z)$.
(3) Set $z_{\mathrm{L}} = z_{\mathrm{L}} + \frac{1}{2^n}\Delta z_{\mathrm{L}}$ with smallest $n \in \{0, 1, 2, \ldots\}$ such that $z_{\mathrm{L}} \in (0, 2)$.
(4) Set $z_{\mathrm{R}} = z_{\mathrm{R}} + \frac{1}{2^n}\Delta z_{\mathrm{R}}$ with smallest $n \in \{0, 1, 2, \ldots\}$ such that $z_{\mathrm{R}} \in (0, 2)$.
(5) Go to Step 1.

References

[1] R. Abgrall and S. Karni, A comment on the computation of non-conservative products. *J. Comput. Phys.* **229** (2010) 2759–2763.

[2] C. Berthon, F. Coquel, J. Hérard and M. Uhlmann, An approximate solution of the Riemann problem for a realisable second-moment turbulent closure. *Shock Waves* **11** (2002) 245–269.

[3] A. Bhole, B. Nkonga, S. Gavrilyuk and K. Ivanova, Fluctuation splitting Riemann solver for a non-conservative modeling of shear shallow water flow. *J. Comput. Phys.* **392** (2019) 205–226.

[4] S. Busto, M. Dumbser, S. Gavrilyuk and K. Ivanova, On thermodynamically compatible finite volume methods and path-conservative ADER discontinuous galerkin schemes for turbulent shallow water flows. *J. Sci. Comput.* **88** (2021) 28.

[5] M.J. Castro, P.G. LeFloch, M.L. Muñoz-Ruiz and C. Parés, Why many theories of shock waves are necessary: convergence error in formally path-consistent schemes. *J. Comput. Phys.* **227** (2008) 8107–8129.

[6] M.J. Castro, C. Parés, G. Puppo and G. Russo, Central schemes for nonconservative hyperbolic systems. *SIAM J. Sci. Comput.* **34** (2012) B523–B558.

[7] M.J. Castro Díaz, A. Kurganov and T. Morales de Luna, Path-conservative central-upwind schemes for nonconservative hyperbolic systems. *ESAIM: M2AN* **53** (2019) 959–985.

[8] J. Cauret, J. Colombeau and A. Le Roux, Discontinuous generalized solutions of nonlinear nonconservative hyperbolic equations. *J. Math. Anal. App.* **139** (1989) 552–573.

[9] P. Chandrashekar, B. Nkonga, A.K. Meena and A. Bhole, A path conservative finite volume method for a shear shallow water model. *J. Comput. Phys.* **413** (2020) 109457.

[10] J.F. Colombeau and A.Y. Le Roux, Multiplications of distributions in elasticity and hydrodynamics. *J. Math. Phys.* **29** (1988) 315–319.

[11] G. Dal Maso, P.G. Lefloch and F. Murat, Definition and weak stability of nonconservative products. *J. Math. Pures Appl.* **74** (1995) 483–548.

[12] M. Dumbser and D.S. Balsara, A new efficient formulation of the HLLEM Riemann solver for general conservative and non-conservative hyperbolic systems. *J. Comput. Phys.* **304** (2016) 275–319.

[13] M. Dumbser, M. Castro, C. Parés and E.F. Toro, ADER schemes on unstructured meshes for nonconservative hyperbolic systems: Applications to geophysical flows. *Comput. Fluids* **38** (2009) 1731–1748.

[14] B. Einfeldt, On Godunov-type methods for gas dynamics. *SIAM J. Numer. Anal.* **25** (1988) 294–318.

[15] S. Gavrilyuk, K. Ivanova and N. Favrie, Multi-dimensional shear shallow water flows: problems and solutions. *J. Comput. Phys.* **366** (2018) 252–280.

[16] S. Gavrilyuk, B. Nkonga, K.-M. Shyue and L. Truskinovsky, Stationary shock-like transition fronts in dispersive systems. Nonlinearity **33** (2020) 5477–5509.

[17] E. Godlewski and P.-A. Raviart, Numerical Approximation of Hyperbolic Systems of Conservation Laws. Vol. 118 of *Applied Mathematical Sciences*. Springer New York, New York, NY (1996).

[18] L. Gosse, A well-balanced scheme using non-conservative products designed for hyperbolic systems of conservation laws with source terms. *Math. Models Methods Appl. Sci.* **11** (2001) 339–365.

[19] K. Joseph and P. Sachdev, Exact solutions for some non-conservative hyperbolic systems. *Int. J. Non-Linear Mech.* **38** (2003) 1377–1386.

[20] P. Lax and B. Wendroff, Systems of conservation laws. *Commun. Pure Appl. Math.* **13** (1960) 217–237.

[21] C.D. Levermore, Moment closure hierarchies for kinetic theories. *J. Stat. Phys.* **83** (1996) 1021–1065.

[22] C.D. Levermore and W.J. Morokoff, The gaussian moment closure for gas dynamics. *SIAM J. Appl. Math.* **59** (1998) 72–96.

[23] C. Parés, Numerical methods for nonconservative hyperbolic systems: a theoretical framework. *SIAM J. Numer. Anal.* **44** (2006) 300–321.

[24] C. Parés and E. Pimentel, The Riemann problem for the shallow water equations with discontinuous topography: the wet – dry case. *J. Comput. Phys.* **378** (2019) 344–365.

[25] K.A. Schneider, J.M. Gallardo, D.S. Balsara, B. Nkonga and C. Parés, Multidimensional approximate Riemann solvers for hyperbolic nonconservative systems. Applications to shallow water systems. *J. Comput. Phys.* **444** (2021) 110547.

[26] V.M. Teshukov, Gas-dynamic analogy for vortex free-boundary flows. *J. Appl. Mech. Tech. Phys.* **48** (2007) 303–309.

[27] E.F. Toro, Shock-Capturing Methods for Free-Surface Shallow Flows. Wiley-Blackwell (2001).

[28] I. Toumi, A weak formulation of roe's approximate riemann solver. *J. Comput. Phys.* **102** (1992) 360–373.

[29] A.I. Volpert, The spaces BV and quasilinear equations. *Math. USSR-Sbornik* **2** (1967) 225–267.